Improving canopy processes in the Community Land Model version 4 (CLM4) using global flux fields empirically inferred from FLUXNET data

Gordon B. Bonan,[1] Peter J. Lawrence,[1] Keith W. Oleson,[1] Samuel Levis,[1] Martin Jung,[2] Markus Reichstein,[2] David M. Lawrence,[1] and Sean C. Swenson[1]

Received 29 October 2010; revised 1 February 2011; accepted 11 February 2011; published 18 May 2011.

[1] The Community Land Model version 4 (CLM4) overestimates gross primary production (GPP) compared with data-driven estimates and other process models. We use global, spatially gridded GPP and latent heat flux upscaled from the FLUXNET network of eddy covariance towers to evaluate and improve canopy processes in CLM4. We investigate differences in GPP and latent heat flux arising from model parameterizations (termed model structural error) and from uncertainty in the photosynthetic parameter $V_{c\ \max}$ (termed model parameter uncertainty). Model structural errors entail radiative transfer, leaf photosynthesis and stomatal conductance, and canopy scaling of leaf processes. Model structural revisions reduce global GPP over the period 1982–2004 from 165 Pg C yr^{-1} to 130 Pg C yr^{-1}, and global evapotranspiration decreases from 68,000 km^3 yr^{-1} to 65,000 km^3 yr^{-1}, within the uncertainty of FLUXNET-based estimates. Colimitation of photosynthesis is a cause of the improvements, as are revisions to photosynthetic parameters and their temperature dependency. Improvements are seen in all regions and seasonally over the course of the year. Similar improvements occur in latent heat flux. Uncertainty in $V_{c\ \max}$ produces effects of comparable magnitude as model structural errors, but of offsetting sign. This suggests that model structural errors can be compensated by parameter adjustment, and this may explain the lack of consensus in values for $V_{c\ \max}$ used in terrestrial biosphere models. Our analyses show that despite inherent uncertainties global flux fields empirically inferred from FLUXNET data are a valuable tool to guide terrestrial biosphere model development and evaluation.

Citation: Bonan, G. B., P. J. Lawrence, K. W. Oleson, S. Levis, M. Jung, M. Reichstein, D. M. Lawrence, and S. C. Swenson (2011), Improving canopy processes in the Community Land Model version 4 (CLM4) using global flux fields empirically inferred from FLUXNET data, *J. Geophys. Res.*, *116*, G02014, doi:10.1029/2010JG001593.

1. Introduction

[2] Models of Earth's land surface, including its terrestrial ecosystems, for climate simulation have expanded beyond their hydrometeorological heritage to include biogeochemical cycles (e.g., carbon and nitrogen), land use, and vegetation dynamics [*Bonan*, 2008]. These models, coupled to their host climate model, are important research tools to study land-atmosphere interactions, climate feedback from ecological processes, and land management practices to mitigate climate change.

[3] The development and evaluation of global terrestrial biosphere models for climate simulation have long utilized eddy covariance tower measurements of energy and carbon fluxes. Such analyses typically involve model calibration and evaluation at one or more flux tower sites [*Morales et al.*, 2005; *Friend et al.*, 2007; *Stöckli et al.*, 2008; *Mercado et al.*, 2009a; *Randerson et al.*, 2009; *Williams et al.*, 2009; *Zaehle and Friend*, 2010; *Mahecha et al.*, 2010] and leave unresolved model evaluation at larger regional to continental scales. However, data-oriented diagnostic techniques to upscale gross primary production (GPP) and latent heat flux from the FLUXNET network of tower sites to global 0.5° gridded data products provide a means to evaluate the models at large scales [*Jung et al.*, 2009, 2010; *Beer et al.*, 2010; M. Jung et al., Global patterns of land-atmosphere fluxes of carbon dioxide, latent heat, and sensible heat derived from eddy covariance, satellite, and meteorological observations, submitted to *Journal of Geophysical Research*, 2011], notwithstanding potential errors in the data products. Here, we use the FLUXNET upscaled GPP and latent heat flux to evaluate and improve canopy processes in one such model, version 4 of the

[1]National Center for Atmospheric Research, Boulder, Colorado, USA.
[2]Max Planck Institute for Biogeochemistry, Jena, Germany.

0148-0227/11/2010JG001593

Table 1. Model Simulations

Simulation	Description
	Model Structural Error
CLM4	control simulation with CLM4
RAD	revised two-stream radiative transfer
RAD-PSN	RAD and revised leaf photosynthesis
RAD-PSN-KN	RAD-PSN and revised canopy scaling (also denoted CLM4a)
	Model Parameter Uncertainty
CLM4a	control simulation (same as RAD-PSN-KN) $V_{c\ \max\ 25} = V_{c\ \max\ 25}^{opt} f(D) f(N)$
OPT	CLM4a with non-nitrogen-limited $V_{c\ \max\ 25}$, $V_{c\ \max\ 25} = V_{c\ \max\ 25}^{opt} f(D)$
KAT	CLM4a with *Kattge et al.* [2009] $V_{c\ \max\ 25}$, $V_{c\ \max\ 25} = V_{c\ \max\ 25}^{Kattge} f(D)$
DAY	CLM4a without day length factor for $V_{c\ \max\ 25}$, $V_{c\ \max\ 25} = V_{c\ \max\ 25}^{opt} f(N)$

Community Land Model (CLM4) [*Oleson et al.*, 2010; *Lawrence et al.*, 2011].

[4] CLM4 substantially overestimates carbon uptake during GPP compared with data-driven estimates and with other models, and the model has a particularly high bias in the tropics [*Beer et al.*, 2010]. We investigate biases in GPP, and associated errors in latent heat flux, arising from model parameterizations (termed model structural error) and from uncertainty in a key model photosynthetic parameter (termed model parameter uncertainty). Model structural errors entail radiative transfer, leaf photosynthesis and stomatal conductance, and canopy scaling of leaf processes. In particular, the distribution of absorbed photosynthetically active radiation among sunlit and shaded portions of the canopy as implemented by *Thornton and Zimmermann* [2007] is theoretically incorrect. CLM4 also simulates high rates of leaf photosynthesis compared with other photosynthesis models, as demonstrated by *Chen et al.* [2010]. We show that revisions to the model to correct these errors substantially improve simulated GPP and latent heat flux compared with the upscaled FLUXNET data.

[5] *Chen et al.* [2010] suggested that the impact of model structural differences can be compensated by parameter adjustment, particularly the photosynthetic parameter $V_{c\ \max}$. This leaf-level parameter describes the maximum rate of carboxylation by the photosynthetic enzyme Rubisco, and other parameters such as the maximum rate of electron transport and leaf maintenance respiration scale with $V_{c\ \max}$ [*Farquhar et al.*, 1980; *Collatz et al.*, 1991, 1992], but estimates of $V_{c\ \max}$ vary greatly and the range of possible values is large, even within a plant functional type [*Wullschleger*, 1993; *Beerling and Quick*, 1995; *Kattge et al.*, 2009]. For example, *Kattge et al.* [2009] derived $V_{c\ \max}$ from a literature synthesis, and those values are much different than the values used in CLM4. We quantify the effect of this parameter uncertainty on simulated GPP and latent heat flux and use the upscaled FLUXNET data to evaluate $V_{c\ \max}$ parameter estimation.

2. Methods

2.1. Model Description

[6] CLM4 continues earlier versions CLM2 [*Bonan et al.*, 2002] and CLM3 [*Oleson et al.*, 2004; *Dickinson et al.*, 2006], and it succeeds CLM3.5 [*Oleson et al.*, 2008; *Stöckli et al.*, 2008] with revised hydrology and snow parameterizations, organic soils, a 50 m deep ground column, and an updated distribution of plant functional types [*Oleson et al.*, 2010; *Lawrence et al.*, 2011]. The model simulates CO_2 assimilation by the plant canopy (GPP) as part of its coupled photosynthesis-stomatal conductance parameterization. Leaf area index for each plant functional type is specified by a globally gridded monthly data set derived from satellite data [*Lawrence et al.*, 2011]. CLM4 includes a biogeochemical parameterization of the terrestrial carbon and nitrogen cycles, in which GPP drives prognostic leaf area and vegetation and soil carbon pools and in which the associated nitrogen cycle constrains carbon fluxes. That version of the model (denoted CLM4CN) has large biases in leaf area [*Lawrence et al.*, 2011]. Here, we do not utilize the carbon-nitrogen biogeochemistry and instead use the prescribed satellite-derived monthly leaf area index so that GPP is unaffected by biases in the CLM4CN biogeochemistry and prognostic leaf area.

[7] For these simulations, a 57 year (1948–2004) meteorological data set was used to force the model in offline simulations uncoupled from a climate model, as in the works of *Oleson et al.* [2008] and *Lawrence et al.* [2011]. Land cover was held constant at values for year 2000, but atmospheric CO_2 varied as in the historical record. The spatial resolution of the model is 1.25 degrees in longitude by 0.9375 degrees in latitude.

2.2. Model Simulations and Test Data

[8] We performed four simulations to document biases arising from model structural errors (Table 1): CLM4, a control simulation with CLM4; RAD, a simulation with revisions to the two-stream radiative transfer parameterization to correctly account for sunlit and shaded leaves (section 2.3); RAD-PSN, as in RAD but with revisions to the leaf photosynthesis and stomatal conductance formulation (section 2.4); and RAD-PSN-KN, as in RAD-PSN but with revised canopy scaling to account for exponential decline in foliage nitrogen concentration with depth in the canopy (section 2.5). This latter simulation is denoted CLM4a to distinguish the full model with all parameterization improvements from CLM4.

[9] We also performed simulations to investigate uncertainty in $V_{c\ \max}$. CLM4 uses a potential value $V_{c\ \max\ 25}^{opt}$ (derived from prescribed, time-invariant foliage nitrogen concentration as described by *Thornton and Zimmermann* [2007]), and this defines the maximum attainable carboxylation rate (adjusted to 25°C). The realized rate (at 25°C) is obtained after adjusting for day length and nitrogen limitation. The expression $V_{c\ \max\ 25} = V_{c\ \max\ 25}^{opt} f(\mathrm{D})$ provides the potential carboxylation rate in the absence of nitrogen limitation, after reduction for day length using the function $f(D) = (D/D_{\max})^2$, where D is day length and $D_{\max}$ is maximum day length. Seasonal changes in photosynthetic capacity have been observed in trees [e.g., *Niinemets et al.*, 1999; *Wilson et al.*, 2000; *Xu and Baldocchi*, 2003], and the CLM4 parameterization assigns this variability to day length [*Oleson et al.*, 2010].

[10] When the carbon-nitrogen biogeochemistry is active, the amount of nitrogen required to support the potential growth is diagnosed, and GPP is reduced if nitrogen

Table 2. Values for $V_{c\,\mathrm{max25}}^{opt}$ (μmol m^{-2} s^{-1})

Plant Functional Type	CLM4		*Kattge et al.* [2009]
	$V_{c\,\mathrm{max}\,25}^{opt}$	$V_{c\,\mathrm{max}\,25}^{opt} f(N)$	$V_{c\,\mathrm{max}\,25}^{Kattge}$
Needleleaf evergreen tree, temperate	61	55	62
Needleleaf evergreen tree, boreal	54	42	62
Needleleaf deciduous tree, boreal	57	29	39
Broadleaf evergreen tree, tropical	72	66	41[a]
Broadleaf evergreen tree, temperate	72	51	61
Broadleaf deciduous tree, tropical	52	36	41[a]
Broadleaf deciduous tree, temperate	52	30	58
Broadleaf deciduous tree, boreal	52	40	58
Broadleaf evergreen shrub, temperate	72	36	62
Broadleaf deciduous shrub, temperate	52	30	54
Broadleaf deciduous shrub, boreal	52	19	54
C_3 grass, arctic	52	21	78
C_3 grass	52	26	78
C_4 grass	52	25	78[b]
Crop	57	31	101

[a]*Kattge et al.* [2009] report a low value of 29 μmol m^{-2} s^{-1}.
[b]Not reported by *Kattge et al.* [2009] and assigned a value for C_3 grass, as in CLM4.

availability is insufficient to sustain the potential biomass increment. Without carbon-nitrogen biogeochemistry (as in our CLM4 simulations reported here), the same formulation is used but $V_{c\,\mathrm{max}\,25}^{opt}$ is reduced by a prescribed nitrogen factor so that $V_{c\,\mathrm{max}\,25} = V_{c\,\mathrm{max}\,25}^{opt} f(D) f(N)$ is the realized value. This ensures that leaf photosynthetic rates (and GPP) are adjusted for nitrogen availability. The term $f(N)$ is scaled between zero and one to represent nitrogen constraints on photosynthesis, varies among plant functional types, and is derived from a CLM4CN simulation [*Bonan and Levis*, 2010].

[11] We performed three simulations (Table 1) to quantify the effects of uncertainty in the CLM4 values of $V_{c\,\mathrm{max}\,25}$, as represented by the terms $V_{c\,\mathrm{max}\,25}^{opt}$, $f(N)$, and $f(D)$. The first simulation examined the term $f(N)$. The inferred nitrogen limitation factors $f(N)$ yield lower values for $V_{c\,\mathrm{max}\,25}$ compared with $V_{c\,\mathrm{max}\,25}^{opt}$ (Table 2), yet both estimates are within the range of published values obtained from synthesis studies [*Wullschleger*, 1993]. Therefore, we performed a CLM4a simulation using the maximum values obtained with $f(N) = 1$ (denoted OPT). The second simulation used the *Kattge et al.* [2009] estimates of $V_{c\,\mathrm{max}\,25}$. *Kattge et al.* [2009] derived $V_{c\,\mathrm{max}\,25}$ based on a synthesis of photosynthetic measurements extrapolated to natural vegetation using observed foliage nitrogen content (Table 2), and we evaluated their performance in CLM4a (denoted KAT). In the third simulation, we removed the CLM4 day length factor so that $V_{c\,\mathrm{max}\,25}$ does not vary through the year (denoted DAY).

[12] We compared model simulations with observationally based GPP and latent heat flux derived from the FLUXNET network of eddy covariance towers. The global FLUXNET upscaling uses data-oriented diagnostic models trained with the eddy covariance flux data to provide empirically derived, spatially gridded fluxes. For this study, the global FLUXNET upscaling utilized the model tree ensembles (MTE) approach, described by *Jung et al.* [2009, also submitted manuscript, 2011] and applied to GPP and latent heat flux [*Beer et al.*, 2010; *Jung et al.*, 2010, also submitted manuscript, 2011]. The upscaling relies on remotely sensed estimates of the fraction of absorbed photosynthetically active radiation (fAPAR), climate, and land cover data. The FLUXNET-MTE upscaling provides monthly fluxes at 0.5° spatial resolution. We regridded the data to the CLM4 grid, excluding FLUXNET-MTE grid cells with no data (typically desert and barren land cover). We analyzed the 23 year period 1982–2004.

2.3. Radiative Transfer

[13] CLM4, and its predecessors, utilizes the two-stream approximation [*Sellers et al.*, 1996a] to calculate radiative transfer and surface albedo for direct beam and diffuse radiation and for visible (<0.7 μm) and near-infrared (≥0.7 μm) wave bands. In CLM4, absorbed photosynthetically active radiation (the visible wave band) is partitioned to sunlit and shaded leaves for photosynthesis [*Thornton and Zimmermann*, 2007]. *Dai et al.* [2004] developed a sunlit and shaded leaf canopy parameterization for the Common Land Model (CoLM) with analytical solutions to the two-stream approximation (Appendix A). CLM4 does not use this solution and instead diagnoses the radiation absorbed by sunlit and shaded leaves from the total radiation absorbed by the canopy.

[14] *Thornton and Zimmermann* [2007] describe the sunlit and shaded leaf parameterization, and *Oleson et al.* [2010] provide the numerical implementation. The direct beam radiation absorbed by the canopy is partitioned into unscattered direct beam and scattered direct beam. Sunlit leaves receive all the unscattered direct beam radiation absorbed by the canopy and additionally a fraction of the total diffuse radiation (scattered direct beam radiation and atmospheric diffuse radiation) absorbed by the canopy. Shaded leaves receive only diffuse radiation. The diffuse radiation absorbed by the canopy is apportioned to sunlit and shaded leaves in relation to the sunlit and shaded fractions of the canopy.

[15] The CLM4 diagnosis of sunlit and shaded leaf radiation differs markedly from the analytical solution of *Dai et al.* [2004] (Figure 1). The two parameterizations are similar in their absorption of direct beam photosynthetically active radiation, but not for diffuse radiation. CLM4 apportions the total canopy absorption of diffuse radiation to sunlit and shaded leaves based on the sunlit and shaded fractions of the canopy. The amount of diffuse radiation absorbed by sunlit leaves declines with leaf area index >~2 m^2 m^{-2}

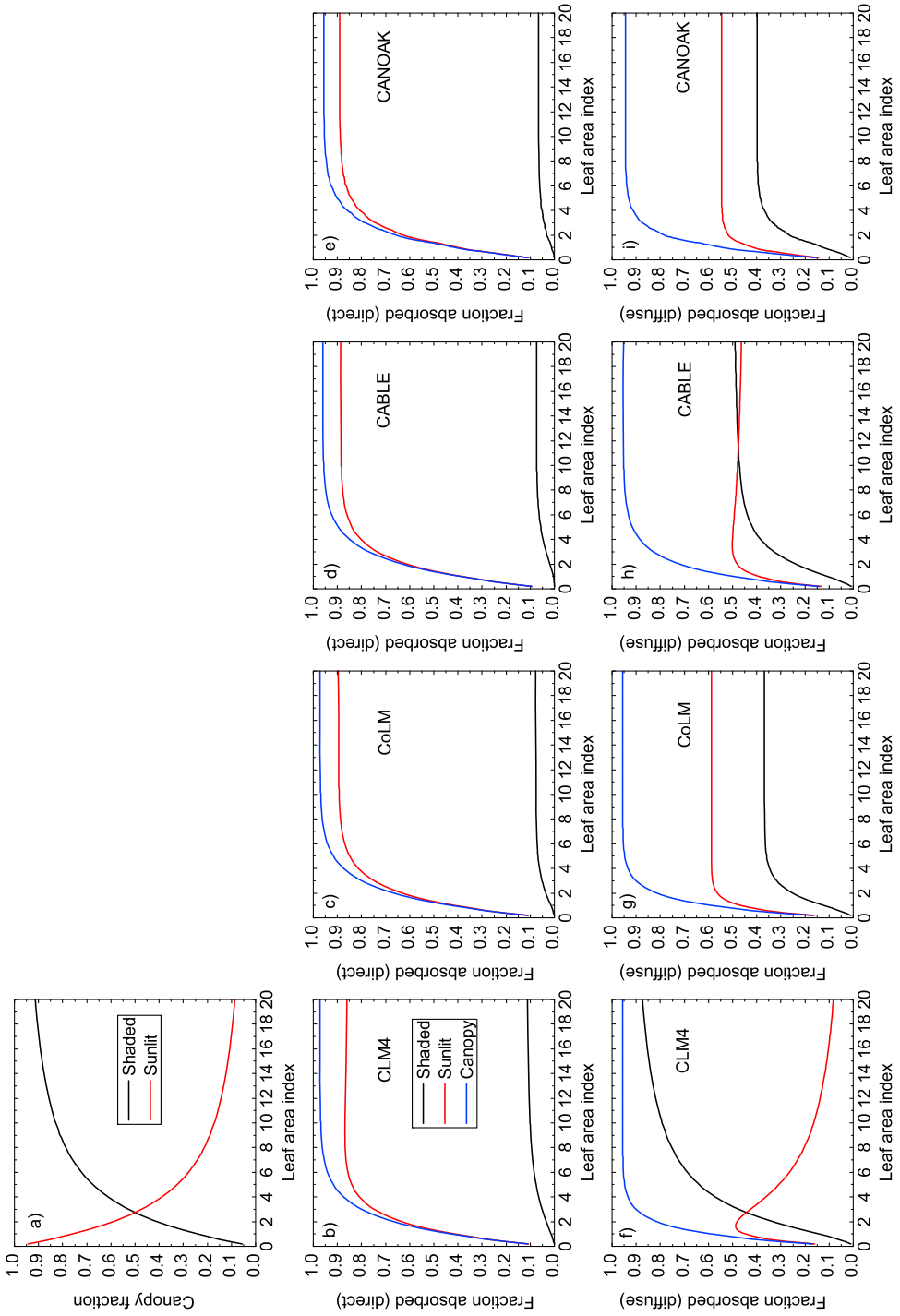

Figure 1. Radiative transfer for photosynthetically active radiation in CLM4 compared with other parameterizations. (a) Fraction of the canopy that is sunlit and shaded in relation to leaf area index. (b-e) Fraction of incident direct beam absorbed by the canopy and by the sunlit and shaded leaves. (f-i) Same as Figures 1b–1e, but for incident diffuse radiation. Shown are the CLM4 two-stream solution [*Thornton and Zimmermann*, 2007]; the *Dai et al.* [2004] analytical two-stream solution implemented in CoLM; the multilayer theory of *Goudriaan* [1977] and *Goudriaan and van Laar* [1994] implemented in the CABLE land surface model [*Kowalczyk et al.*, 2006]; and the multilayer approach of *Norman* [1979] implemented in the CANOAK plant canopy model [*Baldocchi and Wilson*, 2001; *Baldocchi et al.*, 2002]. Simulations are for a canopy of leaves with spherical leaf angle orientation, leaf reflectance of 0.10 and transmittance of 0.05, soil albedo of 0.10, and zenith angle of 30°.

because the sunlit fraction of the canopy declines; and similarly the amount absorbed by shaded leaves increases. The *Dai et al.* [2004] two-stream solution shows near constant absorption for leaf area index greater than ~6 m^2 m^{-2}, and sunlit leaves absorb more diffuse radiation than do shaded leaves.

[16] For comparison, we also considered the multilayer radiative transfer theory of *Goudriaan* [1977] and *Goudriaan and van Laar* [1994], implemented in plant canopy models [e.g., *de Pury and Farquhar*, 1997; *Wang and Leuning*, 1998] and in the CABLE land surface model [*Kowalczyk et al.*, 2006]; and the multilayer approach of *Norman* [1979], implemented in the CANOAK plant canopy model [*Baldocchi and Wilson*, 2001; *Baldocchi et al.*, 2002]. These parameterizations behave similar to the *Dai et al.* [2004] two-stream solution, though the exact partitioning of radiation between sunlit and shaded leaves varies somewhat among the three approaches (Figure 1).

2.4. Leaf Photosynthesis and Stomatal Conductance

[17] CLM4, and its predecessors, utilizes a coupled leaf photosynthesis and stomatal conductance model that is a variant of the Ball-Berry stomatal conductance model [*Ball et al.*, 1987; *Collatz et al.*, 1991], the *Farquhar et al.* [1980] C_3 photosynthesis model as implemented by *Collatz et al.* [1991], and the *Collatz et al.* [1992] C_4 photosynthesis model. *Bonan* [1995] described this parameterization, and the numerical implementation in CLM4 [*Oleson et al.*, 2010] is unchanged from earlier versions of the model [*Bonan*, 1996; *Oleson et al.*, 2004].

[18] We updated the photosynthesis-conductance parameterization based on literature synthesis and to account for theoretical advances since its original implementation, and we denote the new formulation PSN (Appendix B). In particular, CLM4 has higher rates of leaf photosynthesis than a variant of the Farquhar/Ball-Berry/Collatz model used in CoLM [*Chen et al.*, 2010]. This is related in part to colimitation of photosynthesis in CoLM, used also in the C_3 and C_4 models of *Collatz et al.* [1991, 1992] and implemented in the Simple Biosphere model (SiB) [*Sellers et al.*, 1996a, 1996b]. Moreover, the temperature kinetics of Rubisco derived from experimental studies [*Bernacchi et al.*, 2001, 2003; *Leuning*, 2002] is quite different than that implemented in CLM4 and models such as CoLM and SiB. Key parameterization changes introduced in PSN include: colimitation among Rubisco-, light-, and export-limited rates; revised photosynthetic parameters for Rubisco kinetics and their temperature responses; electron transport rate for light-limited photosynthesis with a maximum rate J_{max}; exported-limited photosynthesis based on the rate of triose phosphate utilization; and C_4 photosynthesis similar to *Collatz et al.* [1992] and SiB [*Sellers et al.*, 1996a, 1996b].

[19] The C_3 leaf photosynthetic rates are lower for PSN than for CLM4 (Figure 2). This is related in part to the introduction of colimitation in PSN, noted also in a comparison between the CLM4 and CoLM parameterizations [*Chen et al.*, 2010]. Photosynthetic rates are higher without colimitation (compare PSN with colimitation and PSN* without colimitation). The new parameter values for Rubisco kinetics (K_c, K_o, and Γ_*) further reduce photosynthetic rates (compare CLM4 and PSN*, both without colimitation). Additionally, the electron transport rate used in PSN adds curvature to the light response curve compared with the linear function used in CLM4. In the CO_2 response curve, the reduced export-limited rate used in PSN compared with CLM4 lowers the photosynthetic rate at high CO_2 concentration. The temperature functions lower the optimum temperature for PSN by 5–6°C compared with CLM4.

[20] Colimitation similarly reduces leaf photosynthetic rates in C_4 plants (Figure 2). The CO_2 response curves differ because of the higher CO_2-limited rate (w_e) for C_4 photosynthesis used in PSN compared with CLM4. This causes photosynthesis to saturate at lower CO_2 concentration. It also affects the vapor pressure deficit response, because the rate of photosynthesis is not limited by w_e at the ambient CO_2 concentration used in the simulations (379 ppmv) and thus does not depend on intercellular CO_2 (c_i). Consequently, even though stomata close with greater vapor pressure deficit, photosynthesis is insensitive to vapor pressure deficit. In contrast, the photosynthetic rate is limited by w_e (and thus depends on c_i) at the ambient CO_2 in CLM4 and decreases with higher vapor pressure deficit as stomata close. The temperature optimum is shifted about 2°C warmer in PSN compared with CLM4.

[21] *Chen et al.* [2010] previously compared the CLM4 and CoLM photosynthesis-stomatal conductance models. For reference, we compared our results with similar simulations using the CoLM parameterization (Figure 2). The C_3 light and CO_2 response curves for PSN are similar to CoLM. The PSN temperature response has an optimal temperature about 3°C lower than CoLM. The vapor pressure deficit responses are similar, except when PSN limits the response at high vapor pressure deficit. The CoLM C_4 parameterization produces much lower photosynthetic rates than PSN. CoLM limits the electron transport rate to a value less than $J_{max}/4$, used for both C_3 and C_4 plants. When this limitation is removed (CoLM*), the CoLM photosynthetic rates for C_4 plants are similar to PSN.

2.5. Canopy Integration

[22] *Sellers et al.* [1992] introduced canopy scaling of leaf photosynthesis and stomatal conductance based on gradients of foliage nitrogen in the canopy, and *Sellers et al.* [1996a, 1996b] implemented this parameterization in SiB. The photosynthetic parameter $V_{c\ max}$ varies with leaf nitrogen concentration. The original theory postulated that plants optimally allocate resources to maximize carbon gain such that area-based leaf nitrogen is distributed through the canopy in relation to the time-mean profile of photosynthetically active radiation, but it is now recognized that the nitrogen gradient is shallower than the light gradient [*Hollinger*, 1996; *Carswell et al.*, 2000; *Meir et al.*, 2002; *Niinemets*, 2007; *Lloyd et al.*, 2010].

[23] Many plant canopy models [e.g., *de Pury and Farquhar*, 1997; *Wang and Leuning*, 1998] and terrestrial components of climate models including CoLM [*Dai et al.*, 2004; *Chen et al.*, 2010], GISS [*Friend and Kiang*, 2005], CABLE [*Kowalczyk et al.*, 2006], and O-CN [*Zaehle and Friend*, 2010] now parameterize canopy scaling using concepts of sunlit and shaded leaves in combination with an exponential profile of foliage nitrogen (defined by the decay coefficient K_n). The canopy is divided into sunlit and shaded fractions, and the photosynthesis-conductance parameterization is solved using canopy-integrated parameters derived

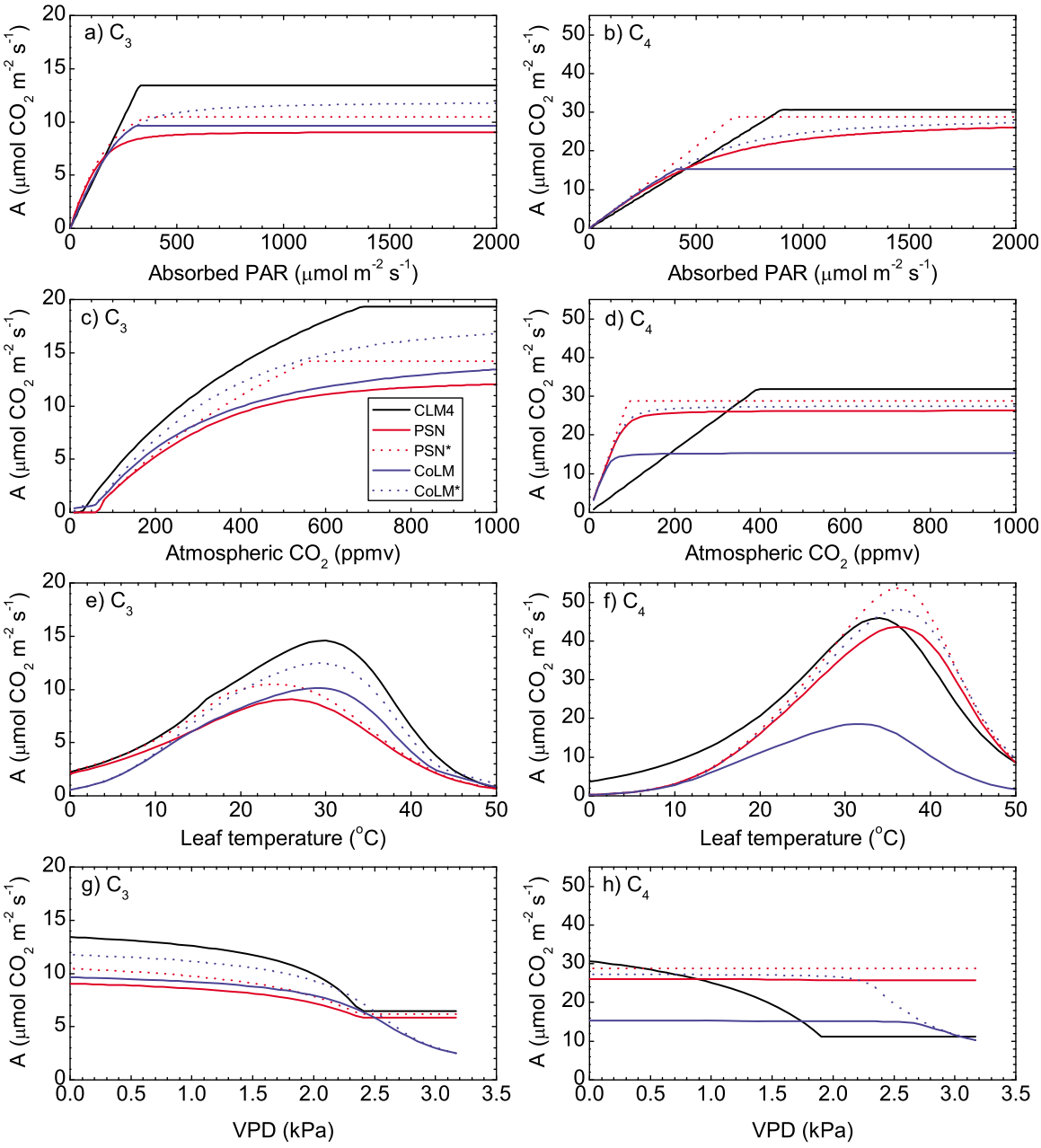

Figure 2. Simulated leaf gross photosynthetic rates for C_3 and C_4 plants. (a and b) Response to absorbed photosynthetically active radiation. (c and d) Response to ambient CO_2 concentration. (e and f) Response to leaf temperature. (g and h) Response to vapor pressure deficit. Shown are the CLM4 solution; the PSN parameterization used in this study; and the PSN parameterization without colimitation (PSN*). As a reference, we show results for CoLM [*Chen et al.*, 2010] with its documented parameterization (CoLM) and with revised electron transport (CoLM*). Reference values are $c_a = 379$ μmol mol^{-1}; $o_i = 0.209$ mol mol^{-1}; P_{atm} = 1013.25 hPa; $\phi = 2000$ μmol photon m^{-2} s^{-1}; $T_v = 25$°C; air temperature is 25°C and relative humidity is 100%; and $g_b = 5$ cm s^{-1}. In these simulations, $V_{c\ \max\ 25} = 40$ μmol m^{-2} s^{-1} (C_3) and 33 μmol m^{-2} s^{-1} (C_4), which are representative values used in CLM4 [*Oleson et al.*, 2010].

from leaf-level parameters. Canopy values for $V_{c\ \max\ 25}$ are found by integrating leaf nitrogen concentration over the sunlit and shaded fractions of the canopy (Appendix C). Other parameters scale similarly.

[24] Values for K_n vary among models, but are generally shallower than the light extinction coefficient. *Friend and Kiang* [2005] reported $K_n = 0.11$ for the GISS model, derived from Amazonia rain forest data [*Carswell et al.*, 2000] and used also in O-CN [*Zaehle and Friend*, 2010]. *Alton et al.* [2007] used $K_n = 0.15$, inferred from measurements in a variety of forests, in simulations of boreal needleleaf forest, temperate broadleaf forest, and Amazonian rain forest with JULES. *Mercado et al.* [2006] derived $K_n = 0.18$ for Amazonian rain forest [*Carswell et al.*, 2000], and

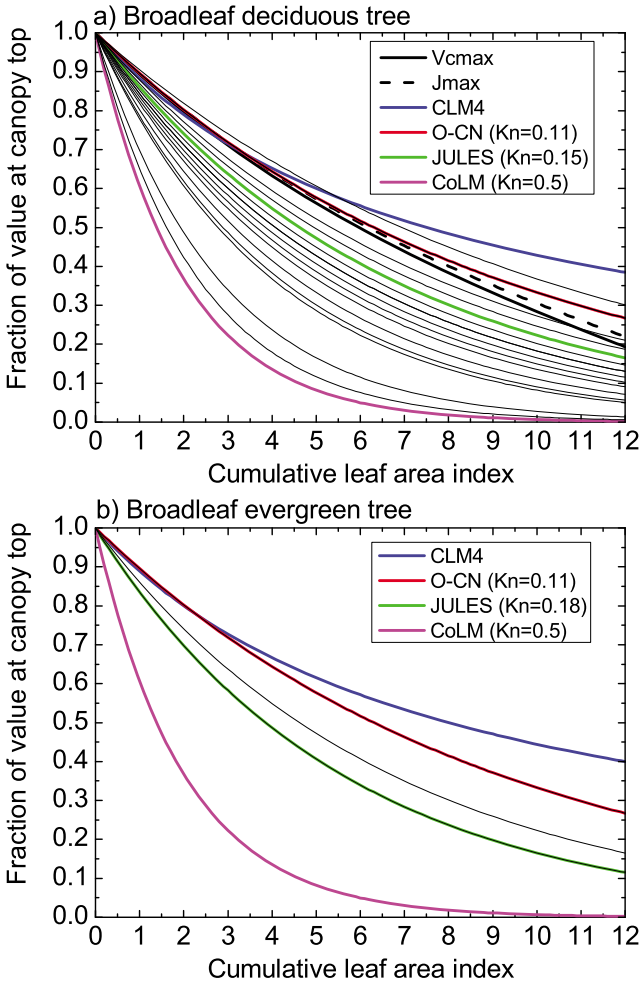

Figure 3. Canopy profiles of $V_{c\ \max}$ (at 25°C) in relation to cumulative leaf area index. (a) Shown are observed profiles for $V_{c\ \max}$ and $J_{\max}$ from *Niinemets and Tenhunen* [1997] obtained for sugar maple (*Acer saccharum*). Also shown are profiles for CLM4 and profiles for K_n equal to 0.11 used in O-CN [*Zaehle and Friend*, 2010], 0.15 used in JULES [*Alton et al.*, 2007], and 0.5 used in CoLM [*Dai et al.*, 2004]. Thin lines show profiles using derived values of K_n for 16 temperate broadleaf forests, ranging from 0.10 to 0.43 [*Lloyd et al.*, 2010]. There are two overlapping values each of 0.11 and 0.17. (b) Shown are $V_{c\ \max}$ profiles for tropical broadleaf evergreen tree for CLM4 and profiles for K_n equal to 0.11 used in O-CN [*Zaehle and Friend*, 2010], 0.18 used in JULES [*Mercado et al.*, 2006], and 0.5 used in CoLM [*Dai et al.*, 2004]. Thin lines show profiles using values of K_n derived from tropical forest observations equal to 0.11 [*Friend and Kiang*, 2005], 0.15 [*Lloyd et al.*, 2010], and 0.18 [*Mercado et al.*, 2006].

Mercado et al. [2009a] used values of 0.16–0.25 (mean, 0.20) for five rain forest sites in the Brazilian Amazon (L. Mercado, personal communication, 2010). Larger values have been used in some models. CoLM uses K_n = 0.5 for $V_{c\ \max}$ scaling and 0.72 for $J_{\max}$ scaling [*Dai et al.*, 2004].

[25] CLM4 uses a comparable scaling approach, but the canopy gradient in foliage nitrogen is specified through a linear decrease in foliage mass per unit leaf area M_a (g C m^{-2}), or an increase in specific leaf area *SLA* (m^2 g^{-1} C), with greater cumulative leaf area from the canopy top [*Thornton and Zimmermann*, 2007]. The gradient is specified such that M_a decreases twofold from canopy top to canopy bottom with a leaf area index of 8 m^2 m^{-2}. Mass-based foliage nitrogen concentration N_m (g N g^{-1} C) is constant with canopy depth, but area-based foliage nitrogen N_a (g N m^{-2}) decreases because M_a decreases with depth ($N_a = N_m\ M_a$). Canopy values for $V_{c\ \max\ 25}$ are found by integrating M_a over the sunlit and shaded fractions of the canopy to obtain sunlit and shaded N_a, from which $V_{c\ \max\ 25}$ is obtained (Appendix C).

[26] While canopy scaling based on gradients of M_a, or conversely *SLA*, may be a useful conceptual framework, its implementation in CLM4 has several limitations. Observational studies find that M_a decreases exponentially with greater depth in forest canopies [*Niinemets and Tenhunen*, 1997; *Meir et al.*, 2002; *Lloyd et al.*, 2010]. Indeed, CLM4 has a shallower gradient in $V_{c\ \max}$ than seen in observations or used in other models (Figure 3). The CLM4 profile of $V_{c\ \max}$ compares favorably with data of *Niinemets and Tenhunen* [1997] for broadleaf deciduous tree at low leaf area, but declines too gradually at high leaf area. In contrast, an exponential profile with K_n = 0.11 [*Friend and Kiang*, 2005; *Zaehle and Friend*, 2010] more closely matches the observations. K_n = 0.15 [*Alton et al.*, 2007] produces a sharper decline, and K_n = 0.50 [*Dai et al.*, 2004] yields a steep decline. *Lloyd et al.*'s [2010] estimates of K_n for 16 temperate broadleaf forests range from 0.10 to 0.43 (mean, 0.20; median, 0.18), all yielding a steeper gradient than in CLM4. The CLM4 profile of $V_{c\ \max}$ for tropical broadleaf evergreen tree is similarly shallower than profiles derived for Amazonian rain forest (K_n = 0.11 [*Friend and Kiang*, 2005]; K_n = 0.15 [*Lloyd et al.*, 2010]; K_n = 0.18 [*Mercado et al.*, 2006]). Large values of $V_{c\ \max}$ at high leaf area may contribute to the model's high GPP bias.

[27] The M_a scaling in CLM4 is limited only to trees; shrubs, grasses, and crops have no canopy scaling. Canopy gradients of N_a related to the M_a profile are commonly observed in forests [*Ellsworth and Reich*, 1993; *Hollinger*, 1996; *Carswell et al.*, 2000; *Meir et al.*, 2002; *Niinemets*, 2007; *Lloyd et al.*, 2010]. Canopy nitrogen gradients have been observed in grasslands [*Schimel et al.*, 1991; *Anten et al.*, 1998] and other herbaceous plant assemblages [*Hirose and Werger*, 1987; *Hirose et al.*, 1988] and also in agricultural crops [*Evans*, 1993; *Dreccer et al.*, 2000; *Drouet and Bonhomme*, 2004; *Gastal and Lemaire*, 2002]. An empirical exponential nitrogen profile allows for gradients in photosynthetic capacity in vegetation where gradients in leaf morphology may not be valid.

[28] As an alternative to the CLM4 canopy scaling, we implemented scaling based on an exponential profile of N_a with K_n = 0.11, as in GISS [*Friend and Kiang*, 2005] and O-CN [*Zaehle and Friend*, 2010]. Our implicit assumption is that this gradient arises from an exponential profile of M_a in trees, but the gradient is unrelated to M_a for other vegetation.

3. Results

[29] CLM4 simulates global GPP equal to 165 Pg C yr^{-1} over the period 1982–2004 (Table 3). For comparison, the

Table 3. Global GPP and Evapotranspiration From Model Simulations[a]

Simulation	GPP (Pg C yr^{-1})	ET (10^3 km^3 yr^{-1})
Observationally Based Estimates		
FLUXNET-MTE, 1982–2004 (this study)	117	-
FLUXNET-MTE, 1982–2008 [*Jung et al.*, 2010, also submitted manuscript, 2011]	119 ± 6	65 ± 3
FLUXNET-diagnostic model ensemble mean, 1998–2005 [*Beer et al.*, 2010]	123 ± 8	-
Model Structural Error		
CLM4	165	68
RAD	155	67
RAD-PSN	132	65
RAD-PSN-KN	130	65
Model Parameter Uncertainty		
CLM4a	130	65
OPT	161	67
KAT	164	67
DAY	142	66

[a]ET, evapotranspiration.

FLUXNET-MTE GPP used in this study is 117 Pg C yr^{-1} over the same period. Jung et al. (submitted manuscript, 2011) estimated GPP to be 119 ± 6 Pg C yr^{-1} for the period 1982–2008 in their analysis using FLUXNET-MTE, and *Beer et al.* [2010] estimated GPP to be 123 ± 8 Pg C yr^{-1} from an ensemble mean of FLUXNET diagnostic models for the period 1998–2005 (95% confidence interval, 102–135 Pg C yr^{-1}). The corrected canopy radiation parameterization (RAD) reduces GPP by 10 Pg C yr^{-1}, and the updated photosynthesis-stomatal conductance formulation decreases GPP by an additional 23 Pg C yr^{-1} (compare RAD-PSN with RAD). The revised canopy scaling has minor effect on GPP (2 Pg C yr^{-1} decrease, compare RAD-PSN-KN with RAD-PSN).

[30] The various values for $V_{c\ \max\ 25}$ change global GPP by a similar magnitude as model structural errors, but with offsetting sign (Table 3). The CLM4 maximum values (OPT) increase GPP by 31 Pg C yr^{-1} compared with CLM4a, and the *Kattge et al.* [2009] values (KAT) increase GPP by 34 Pg C yr^{-1}. Removal of the day length formulation (DAY) increases GPP by 12 Pg C yr^{-1}.

[31] CLM4 overestimates annual GPP compared with FLUXNET-MTE in the tropics and throughout the extratropics (Figures 4 and 5a). Simulated GPP is larger than 5000 g C m^{-2} yr^{-1} throughout regions of tropical rain forest and is approximately 25% greater than FLUXNET-MTE in the midlatitudes (30–60°N). GPP decreases in the RAD simulation, and the RAD-PSN simulation best matches FLUXNET-MTE, especially in the extratropics, though tropical GPP is overestimated. The revised canopy scaling formulation has minor effect (Figures 5a and 6a).

[32] Table 4 shows simulated biome GPP, and this can be compared to *Luyssaert et al.*'s [2007] biome synthesis. CLM4 overestimates tropical evergreen forest GPP (5144 g C m^{-2} yr^{-1}) compared with observationally based estimates of 3551 ± 160 g C m^{-2} yr^{-1} [*Luyssaert et al.*, 2007]. Model revisions reduce GPP to 3654 g C m^{-2} yr^{-1}. Temperate forest GPP (2096 g C m^{-2} yr^{-1}) is high compared to estimates of 1228 ± 286 (semiarid evergreen), 1375 ± 56 (humid deciduous), and 1762 ± 56 (humid evergreen) g C m^{-2} yr^{-1} [*Luyssaert et al.*, 2007], but the revised model (1680 g C m^{-2} yr^{-1}) is more consistent with these estimates. *Luyssaert et al.*'s [2007] GPP for evergreen boreal forest varies from 773 ± 35 (semiarid) to 973 ± 83 (humid) g C m^{-2} yr^{-1}, and increases to 1201 ± 23 g C m^{-2} yr^{-1} for boreal deciduous forest. Boreal forest GPP simulated by the revised model (1029 g C m^{-2} yr^{-1}) is more consistent with these estimates than is CLM4 (1184 g C m^{-2} yr^{-1}). The corrected canopy radiation (RAD) reduces GPP in all biomes, and the updated photosynthesis-conductance (RAD-PSN) produces larger additional decrease in GPP (except for boreal forest and grass).

[33] $V_{c\ \max\ 25}$ parameter uncertainty has substantial effect on annual GPP (Figures 5b and 6b–6d). The *Kattge et al.* [2009] $V_{c\ \max\ 25}$ for tropical broadleaf evergreen trees is lower than that for CLM4 (41 versus 66 μmol m^{-2} s^{-1}, Table 2), and GPP decreases by >500 g C m^{-2} yr^{-1} throughout tropical rain forests. Elsewhere, the *Kattge et al.* [2009] $V_{c\ \max\ 25}$ is larger than CLM4 and GPP increases, in many regions by more than 500 g C m^{-2} yr^{-1}. This is especially prominent in regions of high crop abundance and also grasses ($V_{c\ \max\ 25}$ increases by a factor of three for crops and grasses). However, the increased GPP in tropical savanna is likely a spurious result of our chosen value for C_4 plants (Table 2). The KAT simulation improves annual GPP compared with CLM4a in the tropics, but overestimates GPP in the extratropics. With the exception of tropical trees, the CLM4 non-nitrogen-limited $V_{c\ \max\ 25}$ is comparable to *Kattge et al.* [2009] (compare $V_{c\ \max\ 25}^{Kattge}$ with $V_{c\ \max\ 25}^{opt}$, Table 2) and GPP in the OPT simulation similarly increases compared with CLM4a, though not as much as in the KAT simulation. The effect of day length is smaller in magnitude and is most prominent in middle and high latitudes.

[34] Biome analysis (Table 4) similarly shows that the KAT simulation decreases annual GPP in tropical evergreen forest, but increases GPP elsewhere, especially in crop and tundra. The GPP is comparable to the OPT simulation, with the previously noted exception for tropical evergreen trees. The effect of day length is largest in middle and high latitude biomes.

[35] CLM4 replicates the annual cycle of GPP in arctic, midlatitude, and tropical regions, but is biased high (Figure 7). CLM4a has a similar annual cycle and has reduced mean bias error and root mean square error. The

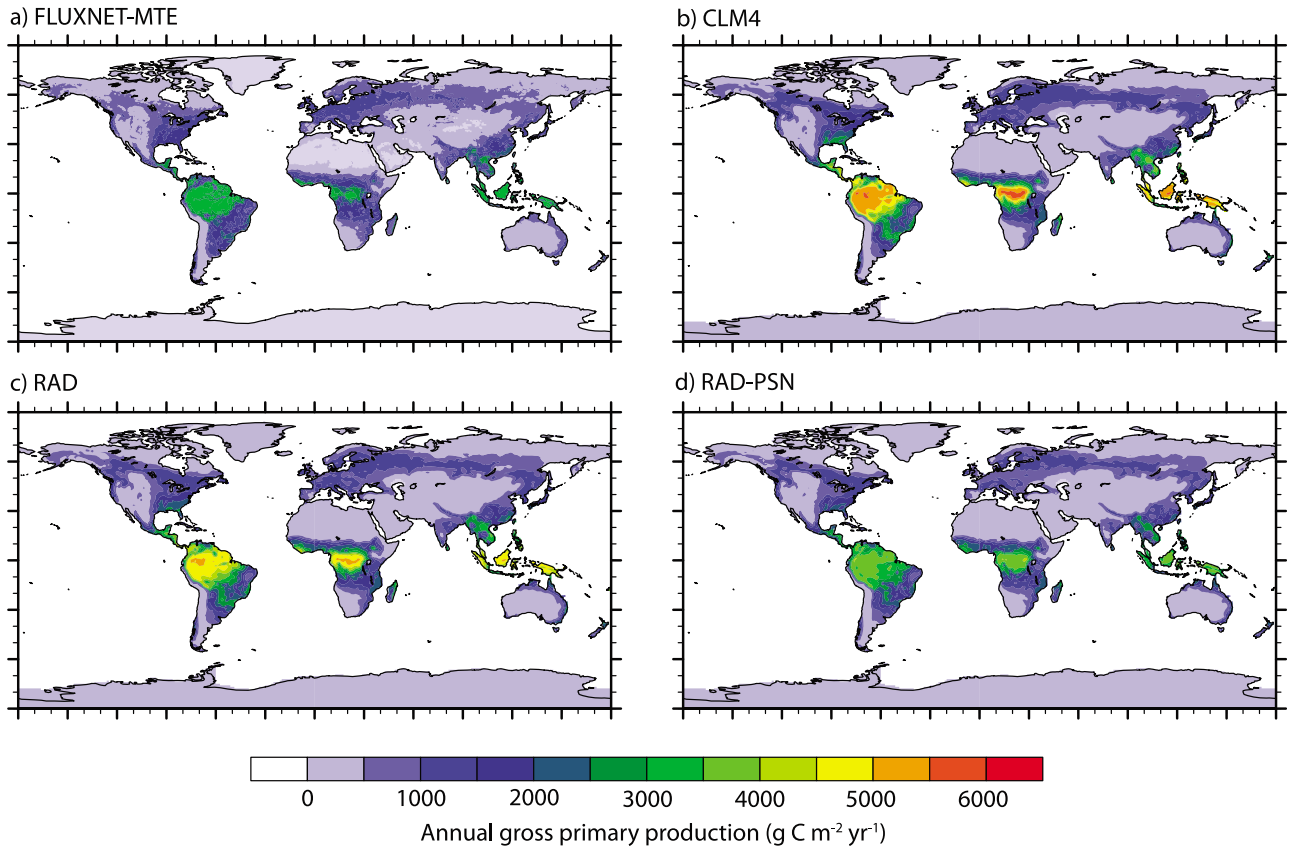

Figure 4. Annual GPP for (a) FLUXNET-MTE and for simulations (b) CLM4, (c) RAD, and (d) RAD-PSN.

effect of day length on $V_{c\ \mathrm{max}\ 25}$ decreases GPP (compare CLM4a with day length and DAY without day length), and this improves the simulated annual cycle in arctic and midlatitude regions. In these regions, the primary effect of day length is to suppress GPP at the end of the growing season.

[36] CLM4 simulates global evapotranspiration equal to 68,000 km^3 yr^{-1} over the period 1982–2004 (Table 3). For comparison, the FLUXNET-MTE evapotranspiration is 65,000 ± 3,000 km^3 yr^{-1} [*Jung et al.*, 2010]. The corrected canopy radiation parameterization (RAD) reduces evapotranspiration by 1,000 km^3 yr^{-1}, and the updated photosynthesis-stomatal conductance (RAD-PSN) decreases evapotranspiration by an additional 2,000 km^3 yr^{-1}. The revised canopy scaling has negligible effect on evapotranspiration. The various values for $V_{c\ \mathrm{max}\ 25}$ change global evapotranspiration by a similar magnitude as model structural errors, but with offsetting sign.

[37] CLM4 overestimates annual latent heat flux compared with FLUXNET-MTE in the tropics, but underestimates latent heat flux in high latitudes (Figures 8 and 9). CLM4a produces a better simulation in the tropics with reduced latent heat flux. The *Kattge et al.* [2009] values for $V_{c\ \mathrm{max}\ 25}$ decrease annual latent heat flux in the tropics and increase latent heat flux in middle and high latitudes.

[38] CLM4a has little effect on monthly latent heat flux compared with CLM4 in arctic regions, but elsewhere reduces latent heat flux during the growing season, improves the simulation, and reduces the root mean square error (Figure 10). The KAT simulation increases growing season latent heat flux in arctic and midlatitude regions compared with CLM4a, but decreases latent heat flux in the Amazon.

4. Discussion

[39] Model structural revisions to CLM4 reduce global GPP over the period 1982–2004 from 165 Pg C yr^{-1} to 130 Pg C yr^{-1}, close to FLUXNET-derived estimates (Table 3). Global annual evapotranspiration decreases from 68,000 km^3 yr^{-1} to 65,000 km^3 yr^{-1}, consistent with FLUXNET estimates. Most of the reduction comes from the updated photosynthesis-stomatal conductance formulation; corrections to canopy radiation have lesser effect; and changes to canopy scaling have minor effect. Improvements to annual GPP are seen in all regions (Figures 4 and 5a) and also in monthly regional fluxes (Figure 7). Associated changes in stomatal conductance produce similar improvements in annual evapotranspiration (Table 3), annual latent heat flux (Figures 8 and 9), and monthly regional latent heat flux (Figure 10). The concomitant improvement in simulated latent heat flux demonstrates the interdependency between photosynthesis and transpiration via stomatal conductance, and it shows the critical importance of ecophysiology and biogeochemistry for surface physics.

[40] Differences between the improved CLM4 and FLUXNET-MTE may be caused by differences in the meteorological forcing and land cover classification. Moreover, the FLUXNET-MTE estimates are statistical estimates with associated uncertainties and subject to other

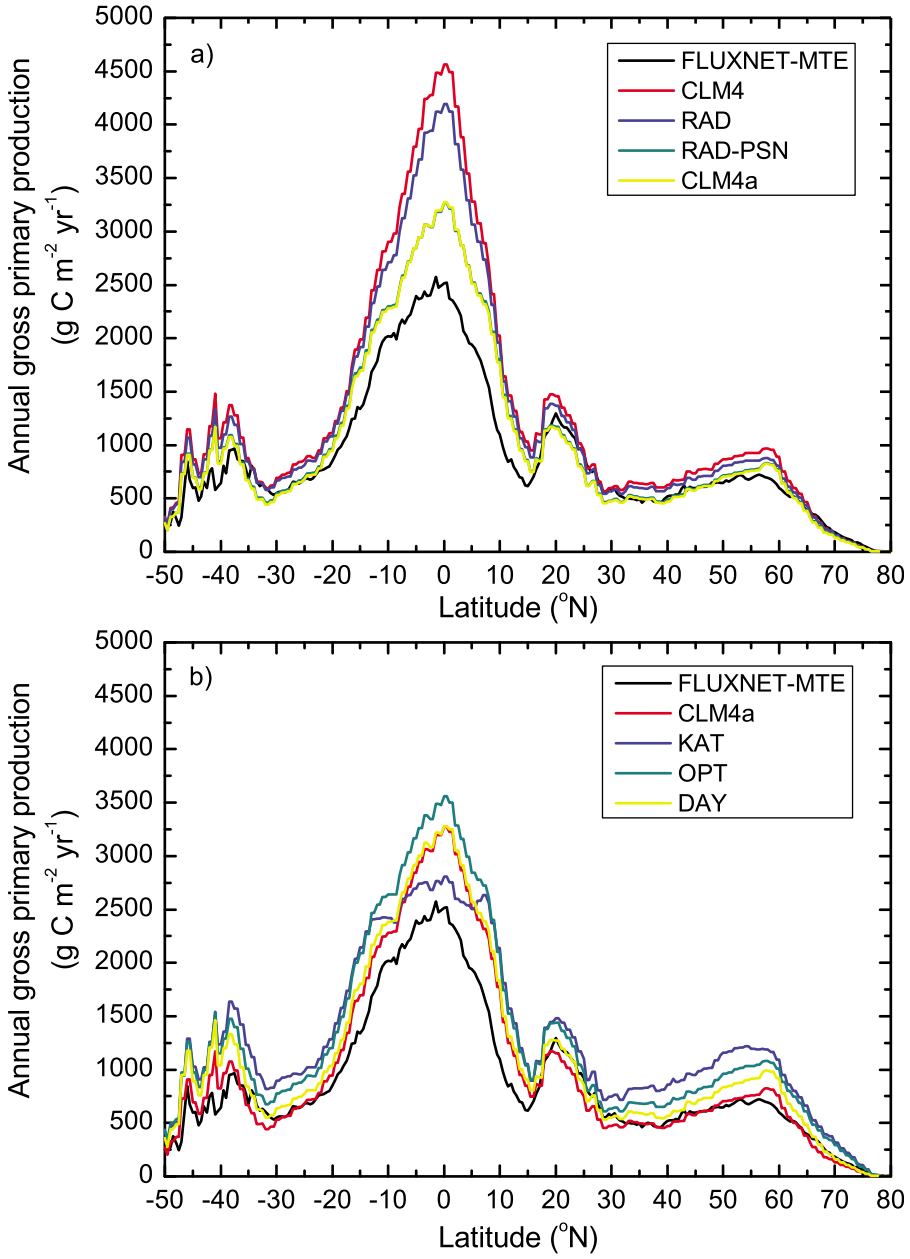

Figure 5. Zonal average annual GPP for (a) model structural error and (b) model parameter uncertainty in comparison with FLUXNET-MTE. Figure 5a shows model structural error for simulations CLM4, RAD, RAD-PSN, and CLM4a (RAD-PSN-KN). Figure 5b shows model parameter uncertainty for simulations KAT, OPT, and DAY in comparison with CLM4a.

errors, e.g., in the underlying eddy covariance data [*Aubinet et al.*, 2000; *Lasslop et al.*, 2010], in global fAPAR retrievals, or through missing factors or predictors in the model tree ensembles (MTE) approach. Such effects have been partly evaluated by *Beer et al.* [2010] from the data-driven modeling perspective and are globally likely below 10 Pg C yr^{-1}, but full uncertainties may be larger and may vary regionally and by season. Nevertheless, it is very likely that the differences between the FLUXNET-MTE estimates and CLM4 simulations exceed this uncertainty and are mainly caused by model structural errors.

[41] Our analyses show that CLM4 biases in GPP arise from model parameterization errors common to both its prescribed, satellite-derived leaf area index and its carbon-nitrogen biogeochemistry with prognostic leaf area. Though not considered here, our results have important implications for simulations of the terrestrial carbon cycle and carbon cycle-climate feedback with carbon-nitrogen biogeochemistry (CLM4CN). The CLM4CN carbon-nitrogen biogeochemistry simulates leaf area index of 12 m^2 m^{-2} or more in many regions of the world [*Lawrence et al.*, 2011]. Our results suggest that this high leaf area may arise in part from too much photosynthetically active radiation absorbed by shaded leaves at high leaf area (Figure 1) and too high values for $V_{c\ max}$ at high leaf area (Figure 3).

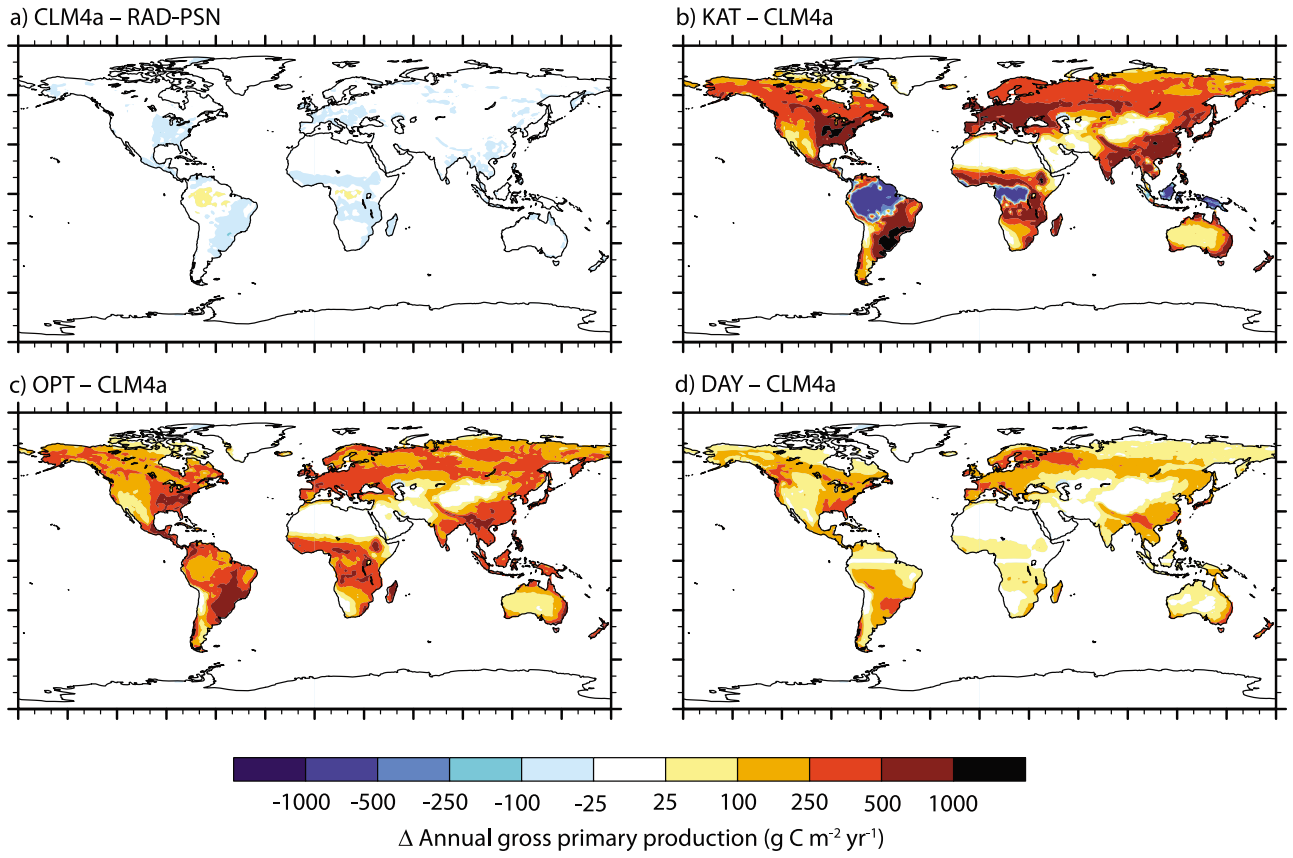

Figure 6. Annual GPP difference for simulations (a) CLM4a (RAD-PSN-KN) compared with RAD-PSN and for (b) KAT, (c) OPT, and (d) DAY compared with CLM4a.

[42] The CLM4 parameterization of radiation absorption by sunlit and shaded leaves is inconsistent with theory (Figure 1). It allows too much absorption of diffuse radiation by shaded leaves, which contributes to the model's high GPP bias, particularly in canopies with high leaf area index. The partitioning of solar radiation between direct beam and diffuse components is an important part of the global carbon cycle and its sensitivity to aerosol forcing [*Mercado et al.*, 2009b]. Our results suggest that CLM4 is overly sensitive to diffuse radiation because of the theoretically incorrect radiative transfer parameterization for sunlit and shaded leaves.

[43] The sensitivity of terrestrial carbon storage to higher atmospheric CO_2 concentration (the CO_2 fertilization response, or concentration-carbon feedback) is an important model metric that differs greatly among coupled carbon cycle-climate models [*Friedlingstein et al.*, 2006]. CLM4 has a higher sensitivity of leaf photosynthesis to CO_2 concentration than does the revised CLM4a, both for C_3 and C_4 plants (Figures 2c and 2d). Carbon cycle simulations with CLM4CN therefore overestimate the concentration-carbon feedback compared with the revised photosynthesis parameterization.

[44] Parameter estimation uncertainty for $V_{c\ \max}$ produces effects of comparable magnitude as model structural errors, but of offsetting sign (Table 3). This suggests that model structural errors can be compensated by parameter adjust-

Table 4. Annual GPP (g C m^{-2} yr^{-1}) by Biome From Model Simulations

Simulation	Tropical Evergreen Forest	Temperate Forest	Boreal Forest	Grass	Crop	Tundra
			Model Structural Error[a]			
CLM4	5,144	2,096	1,184	491	482	185
RAD	4,688 (−9)	1,866 (−11)	1,059 (−11)	490 (0)	477 (−1)	183 (−1)
RAD-PSN	3,634 (−29)	1,684 (−20)	1,028 (−13)	483 (−2)	354 (−27)	160 (−14)
RAD-PSN-KN	3,654 (−29)	1,680 (−20)	1,029 (−13)	472 (−4)	340 (−30)	150 (−19)
			Model Parameter Uncertainty[b]			
CLM4a	3,654	1,680	1,029	472	340	150
OPT	3,902 (7)	2,066 (23)	1,265 (23)	598 (27)	541 (59)	315 (110)
KAT	2,936 (−20)	2,150 (28)	1,376 (34)	663 (40)	788 (132)	348 (132)
DAY	3,728 (2)	1,971 (17)	1,239 (20)	497 (5)	409 (20)	188 (25)

[a]Numbers in parentheses are the percentage deviation from CLM4.
[b]Numbers in parentheses are the percentage deviation from CLM4a.

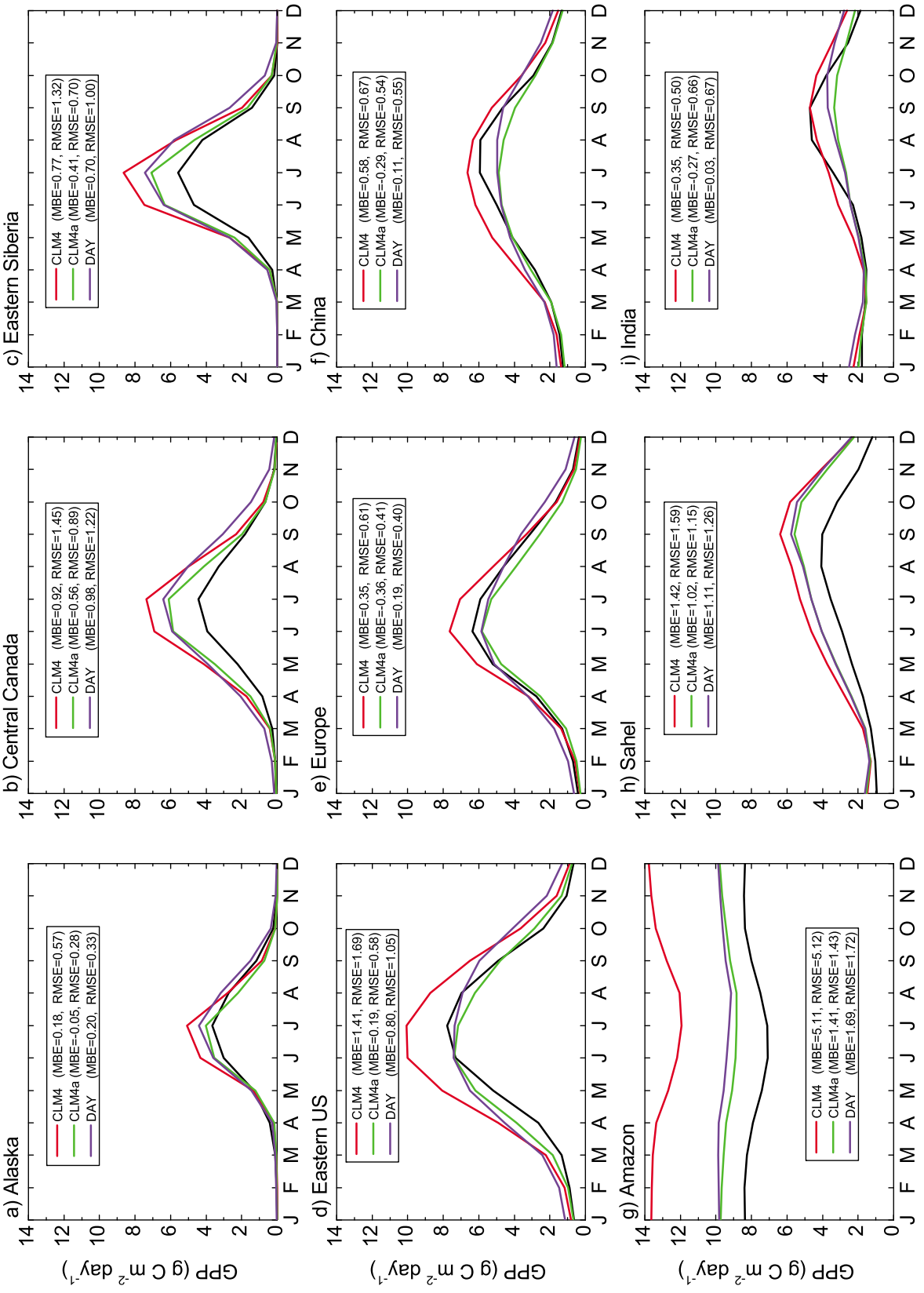

Figure 7. Regional averages of monthly GPP for simulations CLM4, CLM4a, and DAY compared with FLUXNET-MTE. Also shown are mean bias error (MBE) and root mean square error (RMSE).

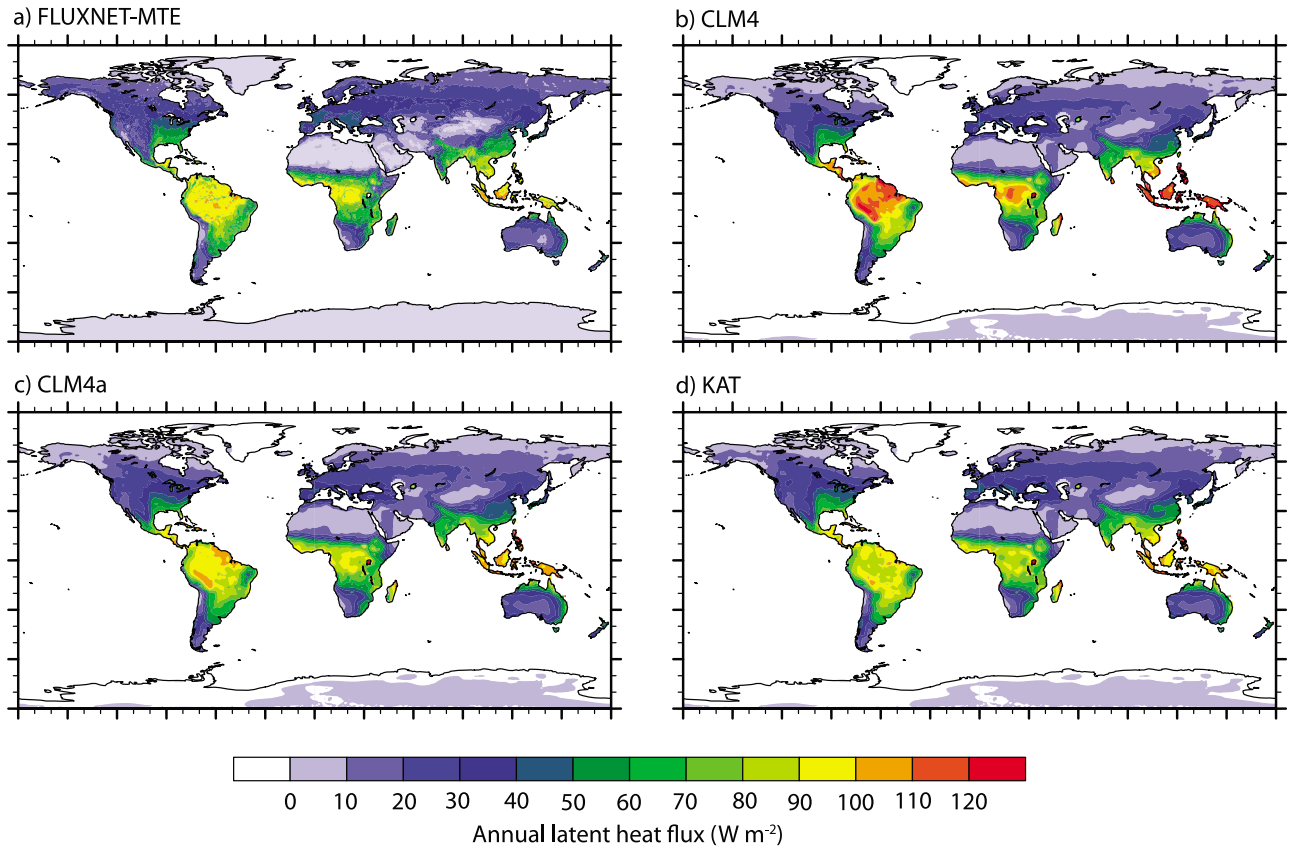

Figure 8. Annual latent heat flux for (a) FLUXNET-MTE and for simulations (b) CLM4, (c) CLM4a, and (d) KAT.

ment, and this may explain the lack of consensus in values for $V_{c\ \max}$ used in terrestrial biosphere models. A particular quandary is that *Kattge et al.* [2009] derived their $V_{c\ \max}$ estimates from a synthesis of photosynthesis studies that they extrapolated to natural vegetation using observed foliage nitrogen concentration. Those parameter values worked well to simulate GPP with the JSBACH vegetation model coupled to the ECHAM5 climate model [*Kattge et al.*, 2009], but degrade GPP (Figures 5b and 6b) and latent heat flux (Figures 9 and 10) in our simulations forced with historical meteorology. It is likely that biases in meteorological forcing and the simulated hydrologic cycle influence the assessment of appropriate $V_{c\ \max}$ values. Until differences among models are resolved, we infer that $V_{c\ \max}$ remains poorly constrained and is likely a model-dependent parameter.

[45] The substantial differences in GPP between the optimal and nitrogen-limited $V_{c\ \max}$ (compare OPT and CLM4a, Table 3 and Figures 5b and 6c) demonstrate the need to properly represent nitrogen's effect on $V_{c\ \max}$. *Kattge et al.* [2009] derived their $V_{c\ \max}$ using extant foliage nitrogen concentrations reported in field studies, but the similarity with CLM4's optimal $V_{c\ \max}$ without nitrogen limitation (compare KAT and OPT, Table 3 and Figure 5b, 6b, and 6c) suggests a key conceptual disparity in how nitrogen is used in CLM4 to constrain GPP. The relationship of $V_{c\ \max}$ to leaf nitrogen concentration is critical to representing the effect of nitrogen availability on GPP, but the CLM4 prescribed, time-invariant $V_{c\ \max}$ precludes leaf nitrogen concentration as a predictor of $V_{c\ \max}$ in relation to nitrogen availability. Models that link $V_{c\ \max}$ with nitrogen availability through prognostic leaf nitrogen concentration retain a fundamental feedback between GPP and nitrogen [e.g., *Zaehle and Friend*, 2010]. Furthermore, the CLM4 use of optimal $V_{c\ \max}$ to calculate GPP, with subsequent reduction in GPP if nitrogen limits productivity, precludes

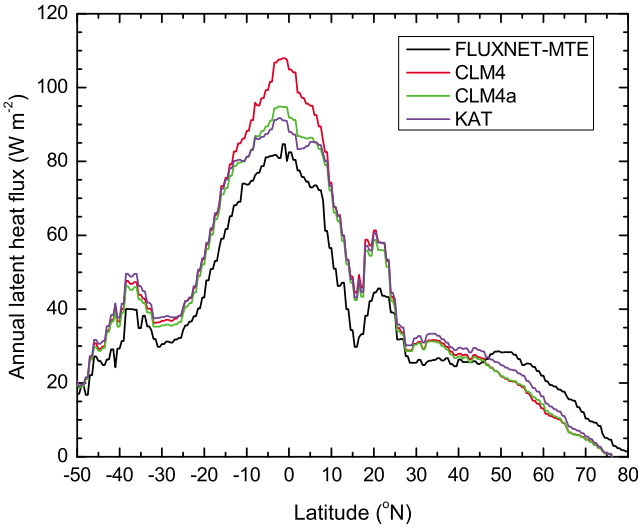

Figure 9. As in Figure 8, but zonal average.

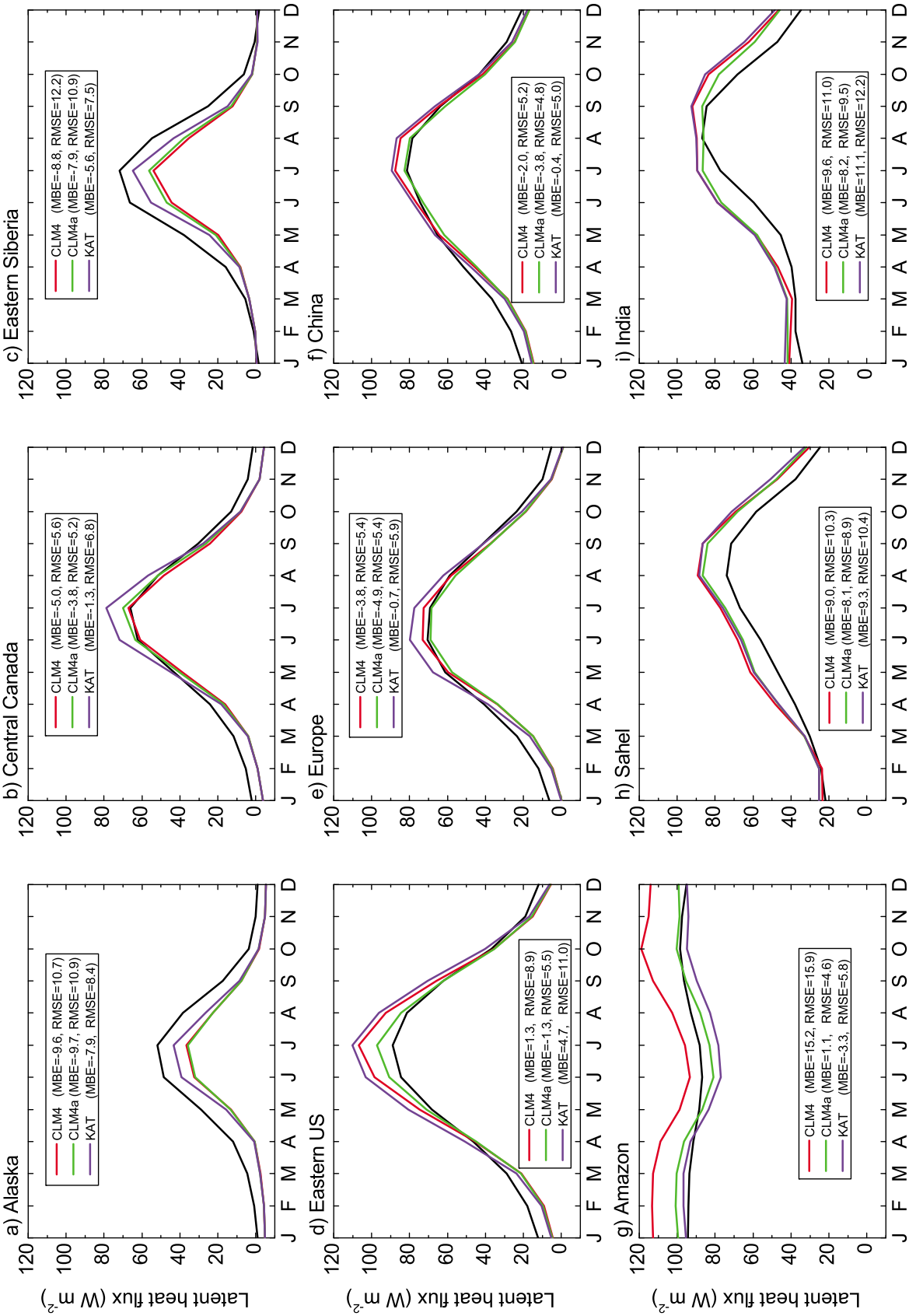

Figure 10. Regional averages of monthly latent heat flux for simulations CLM4, CLM4a, and KAT compared with FLUXNET-MTE. Also shown are mean bias error (MBE) and root mean square error (RMSE).

comparison of model $V_{c\ \max}$ with field and laboratory estimates.

[46] Our results suggest a necessary refinement to $V_{c\ \max}$ parameter estimation for terrestrial biosphere models. The CLM4 day length parameterization suppresses GPP in middle and high latitudes, particularly at the end of the growing season, and this improves the simulated annual cycle (Figure 7). Decreased $V_{c\ \max}$ over the course of the growing season has been observed in many forests [*Dang et al.*, 1998; *Niinemets et al.*, 1999; *Wilson et al.*, 2000; *Xu and Baldocchi*, 2003; *Grassi et al.*, 2005; *Wang et al.*, 2008; *Ow et al.*, 2010], and modeling studies show seasonal trends in carbon fluxes are explained best with temporally varying $V_{c\ \max}$ [*Wilson et al.*, 2001; *Kosugi et al.*, 2003; *Wang et al.*, 2003, 2009a, 2009b]. However, whether this is related to day length as implemented in CLM4 or whether the day length parameterization confounds seasonal changes related to temperature acclimation, soil water stress, or other factors is unclear.

5. Conclusions

[47] Our analyses show that global flux fields empirically inferred from FLUXNET data are a valuable tool to guide terrestrial biosphere model development and evaluation despite the inherent uncertainties in their upscaling. Revisions to CLM4 reduce global GPP over the period 1982–2004 from 165 Pg C yr^{-1} to 130 Pg C yr^{-1} and global evapotranspiration decreases from 68,000 km^3 yr^{-1} to 65,000 km^3 yr^{-1}, both close to FLUXNET-derived estimates. Improvements are seen in all regions and seasonally over the course of the year. Similar improvements occur in latent heat flux through associated changes in stomatal conductance. The updated photosynthesis-stomatal conductance formulation produces the largest effect on GPP and latent heat flux. Colimitation of photosynthesis is a cause of the improvements, as are revisions to photosynthetic parameters and their temperature dependency. Corrections to canopy radiation have lesser effect, and changes to canopy scaling have minor effect. These results have important implications for simulations of the terrestrial carbon cycle, its feedback with climate change, and its sensitivity to aerosols (through diffuse radiation), and they suggest further needed revisions to the model's carbon-nitrogen biogeochemistry.

[48] Uncertainty in the photosynthetic parameter $V_{c\ \max}$ produces effects of comparable magnitude as model structural errors, but of offsetting sign. This suggests that model structural errors can be compensated by parameter adjustment, which may explain the lack of consensus in values for $V_{c\ \max}$ used in terrestrial biosphere models. Dependence on model formulation precludes reliable model intercomparison and parameter refinement. We infer that the photosynthetic parameter $V_{c\ \max}$ remains poorly constrained by observational data and is likely a model-dependent parameter, while ecosystem-level flux observations can be regarded as a model-independent constraint.

Appendix A: Radiative Transfer

[49] *Dai et al.* [2004] provide an analytical solution to the two-stream approximation for sunlit and shaded leaves, and readers are referred to that paper for the theoretical development of these equations. Here, we give their numerical solution. The solution to these equations that follows is from the Common Land Model described by *Dai et al.* [2004], and utilizes the CLM4 two-stream solution described by *Oleson et al.* [2010] to give fluxes per unit incident direct beam and diffuse flux. Our notation uses that of *Oleson et al.* [2010], with the subscript Λ denoting wave band (visible or near-infrared) and the superscript μ denoting direct beam fluxes.

[50] For a canopy with vegetation area index $L' = L + S$ (L, leaf area index; S, stem area index), the solar radiation absorbed by sunlit leaves $\vec{I}^{tot}_{sun,\Lambda}$ (per unit ground area) is

$$\vec{I}^{tot}_{sun,\Lambda} = \int_0^{L'} \left\{ I_{lb,\Lambda}(x) + \left[I_{lbs,\Lambda}(x) + I_{ld,\Lambda}(x) \right] f_{sun}(x) \right\} dx. \quad \text{(A1)}$$

Here, $I_{lb,\Lambda}(x)$ is direct beam radiation that is absorbed; $I_{lbs,\Lambda}(x)$ is direct beam that is scattered and absorbed as diffuse radiation; $I_{ld,\Lambda}(x)$ is diffuse radiation that is absorbed; and

$$f_{sun}(x) = e^{-K_b x} \quad \text{(A2)}$$

is the sunlit fraction at a depth in the canopy with cumulative vegetation area index x, with K_b the direct beam extinction coefficient. The solar radiation absorbed by shaded leaves $\vec{I}^{tot}_{sha,\Lambda}$ (per unit ground area) is

$$\vec{I}^{tot}_{sha,\Lambda} = \int_0^{L'} \left\{ \left[I_{lbs,\Lambda}(x) + I_{ld,\Lambda}(x) \right] \left[1 - f_{sun}(x) \right] \right\} dx. \quad \text{(A3)}$$

The direct beam radiation at depth x that is absorbed (per unit leaf area) is

$$I_{lb,\Lambda}(x) = S_{atm}\ \downarrow^{\mu}_{\Lambda} (1 - \omega_{\Lambda}) K_b e^{-K_b x} \quad \text{(A4)}$$

where $S_{atm}\ \downarrow^{\mu}_{\Lambda}$ is the incident direct beam radiation above the canopy and ω_{Λ} is the leaf scattering coefficient. The scattered direct beam radiation absorbed (per unit leaf area) is

$$I_{lbs,\Lambda}(x) = S_{atm}\ \downarrow^{\mu}_{\Lambda} \left[\omega_{\Lambda} K_b e^{-K_b x} + \frac{d\left(I\uparrow^{\mu}_{\Lambda} - I\downarrow^{\mu}_{\Lambda} \right)}{dx} \right] \quad \text{(A5)}$$

where $I\uparrow^{\mu}_{\Lambda}$ and $I\downarrow^{\mu}_{\Lambda}$ are the two-stream upward and downward scattered fluxes for direct beam. The diffuse radiation absorbed (per unit leaf area) is

$$I_{ld,\Lambda}(x) = S_{atm}\ \downarrow_{\Lambda} \left[\frac{d(I\uparrow_{\Lambda} - I\downarrow_{\Lambda})}{dx} \right] \quad \text{(A6)}$$

where $S_{atm}\ \downarrow_{\Lambda}$ is the incident diffuse radiation above the canopy and $I\uparrow_{\Lambda}$ and $I\downarrow_{\Lambda}$ are the two-stream upward and downward fluxes for diffuse radiation.

[51] The solution to these equations follows *Oleson et al.* [2010, equations (3.1)–(3.47)] and parameters $\overline{\mu}$, s_1, s_2, σ, h, and h_1–h_{10}, with fluxes defined per unit incident direct beam or diffuse radiation above the canopy. The absorption of direct beam radiation by sunlit leaves (per unit ground area) is

$$\vec{I}^{\mu}_{sun,\Lambda} = (1 - \omega_{\Lambda}) \left[1 - s_2 + \frac{1}{\overline{\mu}} (a_1 + a_2) \right] \quad \text{(A7)}$$

Table B1. Equations for the Coupled Photosynthesis-Stomatal Conductance Model

Definition	PSN	CLM4
Stomatal conductance	$g_s = m\frac{A_n}{c_s/P_{atm}}h_s + b\ \beta_t$	$g_s = m\frac{A}{c_s/P_{atm}}h_s + b$
Net photosynthesis	$A_n = A - R_d$	-
Gross photosynthesis	$\Theta_{cj}w_i^2 - (w_c + w_j)w_i + w_c w_j = 0$ $\Theta_{ie}A^2 - (w_i + w_e)A + w_i w_e = 0$	$A = \min(w_c, w_j, w_e)$
Leaf surface CO_2 partial pressure	$c_s = c_a - \frac{1.4}{g_b}A_n\ P_{atm}$	$c_s = c_a - \frac{1.37}{g_b}A\ P_{atm}$
Intercellular CO_2 partial pressure	$c_i = c_s - \frac{1.6}{g_s}A_n\ P_{atm}$	$c_i = c_s - \frac{1.65}{g_s}A\ P_{atm}$
Leaf surface humidity	$h_s = \frac{e_s}{e_*[T_v]} = \frac{g_b e_a + g_s e_*[T_v]}{(g_b+g_s)e_*[T_v]}$ $C_3 : e_a > 0.25e_*[T_v]$ $C_4 : e_a > 0.40e_*[T_v]$	same

and for shaded leaves,

$$\vec{I}^{\mu}_{sha,\Lambda} = \vec{I}^{\mu}_{\Lambda} - \vec{I}^{\mu}_{sun,\Lambda} \tag{A8}$$

with

$$a_1 = \frac{h_1}{\sigma}\left[\frac{1-s_2^2}{2K_b}\right] + h_2\left[\frac{1-s_2 s_1}{K_b+h}\right] + h_3\left[\frac{1-s_2/s_1}{K_b-h}\right] \tag{A9}$$

$$a_2 = \frac{h_4}{\sigma}\left[\frac{1-s_2^2}{2K_b}\right] + h_5\left[\frac{1-s_2 s_1}{K_b+h}\right] + h_6\left[\frac{1-s_2/s_1}{K_b-h}\right]. \tag{A10}$$

Here, $\vec{I}^{\mu}_{\Lambda}$ is the direct beam radiation absorbed by the canopy, from *Oleson et al.* [2010, equation (4.1)]. For diffuse radiation, the absorbed radiation (per unit ground area) for sunlit leaves is

$$\vec{I}_{sun,\Lambda} = \left[\frac{1-\omega_{\Lambda}}{\overline{\mu}}\right](a_1 + a_2) \tag{A11}$$

and for shaded leaves,

$$\vec{I}_{sha,\Lambda} = \vec{I}_{\Lambda} - \vec{I}_{sun,\Lambda} \tag{A12}$$

with

$$a_1 = h_7\left[\frac{1-s_2 s_1}{K_b+h}\right] + h_8\left[\frac{1-s_2/s_1}{K_b-h}\right] \tag{A13}$$

$$a_2 = h_9\left[\frac{1-s_2 s_1}{K_b+h}\right] + h_{10}\left[\frac{1-s_2/s_1}{K_b-h}\right]. \tag{A14}$$

Here, $\vec{I}_{\Lambda}$ is the diffuse radiation absorbed by the canopy, from *Oleson et al.* [2010, equation (4.2)].

[52] The absorbed photosynthetically active (visible wave band) radiation averaged over the sunlit canopy (per unit leaf area) is

$$\phi_{sun} = \left(\vec{I}^{\mu}_{sun,vis}S_{atm}\downarrow^{\mu}_{vis} + \vec{I}_{sun,vis}S_{atm}\downarrow_{vis}\right)\left[\frac{L}{L+S}\right]\Big/ L_{sun} \tag{A15}$$

and the absorbed radiation for the average shaded leaf (per unit leaf area) is

$$\phi_{sha} = \left(\vec{I}^{\mu}_{sha,vis}S_{atm}\downarrow^{\mu}_{vis} + \vec{I}_{sha,vis}S_{atm}\downarrow_{vis}\right)\left[\frac{L}{L+S}\right]\Big/ L_{sha} \tag{A16}$$

with L_{sun} and L_{sha} the sunlit and shaded leaf area index, respectively. The term $L/(L+S)$ is the fraction of the canopy represented by leaf area. The sunlit leaf area index is

$$L_{sun} = \int_0^L f_{sun}(x)\,dx = \frac{1-e^{-K_b L}}{K_b} \tag{A17}$$

and the shaded leaf area index is $L_{sha} = L - L_{sun}$.

Appendix B: Leaf Photosynthesis and Stomatal Conductance

[53] Table B1 lists the equations used in the coupled photosynthesis-conductance model. We use the Ball-Berry stomatal conductance model [*Ball et al.*, 1987; *Collatz et al.*, 1991] as implemented in SiB [*Sellers et al.*, 1996a, 1996b]. This differs from CLM4 in its use of net photosynthesis A_n (after accounting for dark respiration) instead of gross photosynthesis A. The CLM4 use of A rather than A_n for stomatal conductance, leaf surface CO_2 and intercellular CO_2 calculations is theoretically incorrect. Additionally, soil water influences stomatal conductance directly by multiplying the minimum conductance by the CLM4 soil water stress function β_t and also indirectly through A_n in the C_3 and C_4 photosynthesis models [*Sellers et al.*, 1996a, 1996b]. We use colimitation as described by *Collatz et al.* [1991, 1992] and implemented in SiB [*Sellers et al.*, 1996a, 1996b]. Values are $\Theta_{cj} = 0.98$ and $\Theta_{ie} = 0.95$ for C_3 plants; and $\Theta_{cj} = 0.80$ and $\Theta_{ie} = 0.95$ for C_4 plants. In contrast, CLM4 uses the *Farquhar et al.* [1980] minimum limiting rate. In calculating leaf surface humidity, we retain the CLM4 lower limit to canopy air vapor pressure to prevent numerical instability at low humidity.

[54] Table B2 lists equations in the C_3 photosynthesis model. The Rubisco-limited assimilation rate w_c and light-limited assimilation rate w_j are from the *Farquhar et al.* [1980] model. Light-limited assimilation depends on the electron transport rate J, while CLM4 uses the *Collatz et al.* [1991] and SiB [*Sellers et al.*, 1996a, 1996b] dependence on quantum yield ($\varepsilon = 0.06$ mol CO_2 mol^{-1} photon). Subsequent versions of the *Farquhar et al.* [1980] model introduced a third rate w_e limited by the capacity to export or utilize the products of photosynthesis [*Harley and Sharkey*, 1991; *Harley et al.*, 1992; *von Caemmerer*, 2000]. We use the *Harley et al.* [1992] formulation, in contrast to the *Collatz et al.* [1991] approximation used in SiB [*Sellers et al.*, 1996a, 1996b] and CLM4. Soil water stress is

Table B2. Equations for the C_3 Photosynthesis Model

Definition	PSN	CLM4
Rubisco-limited assimilation	$w_c = \frac{V_{c\,\max}\left(c_i-\Gamma_*\right)}{c_i+K_c(1+o_i/K_o)}$	same
Light-limited assimilation	$w_j = \frac{J}{4}(\frac{c_i-\Gamma_*}{c_i+2\Gamma_*})$	$w_j = \varepsilon\ (4.6\phi)[\frac{c_i-\Gamma_*}{c_i+2\Gamma_*}]$ sunlit leaf : $\phi = \phi_{sun}$ shaded leaf : $\phi = \phi_{sha}$
Export-limited assimilation rate	$w_e = 3TPU$	$w_e = 0.5\ V_{c\,\max}$
Electron transport rate	$\Theta_{PSII}J^2 - (I_{PSII} + J_{\max})J + I_{PSII}J_{\max} = 0$	-
Light absorbed by photosystem II	$I_{PSII} = 0.5(1-f)(4.6\phi)$ sunlit leaf : $\phi = \phi_{sun}$ shaded leaf : $\phi = \phi_{sha}$	-
Maximum carboxylation rate	$V_{c\,\max} = V_{c\,\max\,25}\, f(T_v) f_H\,(T_v)\beta_t$	$V_{c\,\max} = V_{c\,\max\,25}\, f(T_v) f_H\,(T_v)\beta_t$
Maximum electron transport rate	$J_{\max} = J_{\max\,25}\, f(T_v) f_H\,(T_v)$	-
Triose phosphate utilization	$TPU = TPU_{25}\, f(T_v) f_H\,(T_v)$	-
Leaf dark respiration	$R_d = R_{d25}\, f(T_v) f_H\,(T_v)\beta_t$	-
Michaelis-Menten constant, CO_2	$K_c = K_{c25}\, f(T_v)$	$K_c = K_{c25}\, f(T_v)$
Michaelis-Menten constant, O_2	$K_o = K_{o25}\, f(T_v)$	$K_o = K_{o25}\, f(T_v)$
CO_2 compensation point	$\Gamma_* = \Gamma_{*25}\, f(T_v)$	$\Gamma_* = 0.5\frac{K_c}{K_o}0.21o_i$
Temperature function	$f(T_v) = \exp\left[\frac{\Delta H_a}{298.15R_{gas}}\left(1-\frac{298.15}{T_v}\right)\right]$	$f(T_v) = Q_{10}^{(T_v-298.15)/10}$
High temperature inhibition	$f_H\,(T_v) = \frac{1+\exp\left(\frac{298.15\Delta S-\Delta H_d}{298.15R_{gas}}\right)}{1+\exp\left(\frac{\Delta ST_v-\Delta H_d}{R_{gas}T_v}\right)}$	$f_H(T_v) = \left[1+\exp\left(\frac{\Delta ST_v-\Delta H_d}{R_{gas}T_v}\right)\right]^{-1}$

applied to $V_{c\,\max}$ and R_d, as in SiB [*Sellers et al.*, 1996a, 1996b].

[55] The electron transport rate J is related to absorbed photosynthetically active radiation, but the equation varies among models. We use a common form from *von Caemmerer* [2000], used also in the plant canopy models of *de Pury and Farquhar* [1997], *Wittig et al.* [2005], and *Mercado et al.* [2009a]. The photosynthetically active radiation varies between sunlit leaves (ϕ_{sun}) and shaded leaves (ϕ_{sha}). For photosynthesis, radiation units are converted from W m^{-2} to μmol photon m^{-2} s^{-1} assuming 4.6 μmol J^{-1}.

[56] CLM4 uses the *Collatz et al.* [1991] and *Sellers et al.* [1996a, 1996b] Q_{10} temperature functions for photosynthetic parameters. We use the Arrhenius function and the *Bernacchi et al.* [2001, 2003] estimates for activation energy ΔH_a (*Harley et al.* [1992] provide ΔH_a for *TPU*). Thermal breakdown of metabolic processes is included by multiplying $V_{c\,\max}$ and $J_{\max}$ by a high temperature stress function [*Leuning*, 2002], which we similarly apply to *TPU* and R_d.

[57] Table B3 lists parameter values for C_3 plants. Values for m and b are from *Sellers et al.* [1996a, 1996b]. CLM4 has a lower value for b, and m varies for needleleaf trees. K_c, K_o, and Γ_* at 25°C are from *Bernacchi et al.* [2001]. $J_{\max}$ varies with $V_{c\,\max}$ in near constant proportion across plant species [*Wullschleger*, 1993], and we use $J_{\max\,25} = 1.97V_{c\,\max\,25}$. Similarly, we use $TPU_{25} = 0.06\ J_{\max\,25}$, also from *Wullschleger* [1993]. We use the *Collatz et al.* [1991] and SiB [*Sellers et al.*, 1996a, 1996b] expression for R_{d25}.

[58] *Collatz et al.* [1992] give corresponding equations for C_4 plants, implemented in SiB [*Sellers et al.*, 1996a, 1996b]. The CLM4 C_4 photosynthesis model does not use these equations, and we update the model for these equations (Table B4). Values of $m = 4$ and $b = 40000$ μmol H_2O m^{-2} s^{-1} are from SiB [*Sellers et al.*, 1996a, 1996b]. Corresponding values in CLM4 are $m = 5$ and $b = 2000$ μmol H_2O m^{-2} s^{-1}. We use quantum yield $\varepsilon = 0.05$ mol mol^{-1} [*Sellers et al.*, 1996a, 1996b], in contrast to $\varepsilon = 0.04$ in CLM4. The temperature functions for $V_{c\,\max}$ and R_d are from SiB [*Sellers et al.*, 1996a, 1996b], as is R_{d25}. In contrast, CLM4 does not distinguish the temperature dependence of $V_{c\,\max}$ between C_3 and C_4 plants. Soil water stress is applied to $V_{c\,\max}$ and R_d similar to C_3 plants. *Sellers et al.* [1996a, 1996b] use $k_e = 20000\ V_{c\,\max}$ (at 25°C) to calculate CO_2-limited assimilation and adjust this for temperature with a Q_{10} function. In contrast, CLM4 uses $k_e = 4000\ V_{c\,\max}$ and k_e follows the environmental response of $V_{c\,\max}$.

[59] The maximum rate of carboxylation varies with foliage nitrogen [*Thornton and Zimmermann*, 2007; *Oleson et al.*, 2010]:

$$V_{c\,\max 25}^{opt} = (N_m M_a) F_{LNR} F_{NR} a_{R25} \tag{B1}$$

where $N_m M_a$ is the area-based leaf nitrogen (g N [leaf] m^{-2} [leaf]) specified from mass-based leaf nitrogen N_m (g N [leaf] g^{-1} C [leaf]) and foliage mass per unit leaf area M_a (g C [leaf] m^{-2} [leaf]; the inverse of specific leaf area); F_{LNR} is the fraction of leaf nitrogen in Rubisco (g N [Rubisco] g^{-1} N [leaf]); $F_{NR} = 7.16$ is the mass ratio of Rubisco to nitrogen in Rubisco (g Rubisco g^{-1} N [Rubisco]); and $a_{R25} = 60$ is the specific activity of Rubisco at 25°C (μmol CO_2 g^{-1} Rubisco s^{-1}). The realized value for $V_{c\,\max\,25}$ is

Table B3. Parameter Values for the C_3 Photosynthesis Model

	PSN		
Parameter	Value (25°C)	Temperature Dependence	CLM4
m	9	-	$m = 9$ $m = 6$(needleleaf tree)
b	10,000 μmol H_2O m^{-2} s^{-1}	-	b = 2,000 μmol H_2O m^{-2} s^{-1}
$V_{c\ \max}$	$V_{c\ \max\ 25} = V_{c\ \max\ 25}^{opt}\, f(D) f(N)$	ΔH_a = 65,330 J mol^{-1} ΔH_d = 149,250 J mol^{-1} ΔS = 485 J mol^{-1} K^{-1}	Q_{10} = 2.4 ΔH_d = 220,000 J mol^{-1} ΔS = 710 J mol^{-1} K^{-1}
$J_{\max}$	$J_{\max\ 25} = 1.97 V_{c\ \max\ 25}$	ΔH_a = 43,540 J mol^{-1} ΔH_d = 152,040 J mol^{-1} ΔS = 495 J mol^{-1} K^{-1}	-
TPU	$TPU_{25} = 0.06 J_{\max\ 25}$	ΔH_a = 53,100 J mol^{-1} ΔH_d = 150,650 J mol^{-1} ΔS = 490 J mol^{-1} K^{-1}	-
R_d	$R_{d25} = 0.015 V_{c\ \max\ 25}$	ΔH_a = 46,390 J mol^{-1} ΔH_d = 150,650 J mol^{-1} ΔS = 490 J mol^{-1} K^{-1}	-
K_c	K_{c25} = 404.9 μmol mol^{-1} (41 Pa at 1,013.25 hPa)	ΔH_a = 79,430 J mol^{-1}	K_{c25} = 30 Pa Q_{10} = 2.1
K_o	K_{o25} = 278.4 mmol mol^{-1} (28,209 Pa at 1,013.25 hPa)	ΔH_a = 36,380 J mol^{-1}	K_{o25} = 30,000 Pa Q_{10} = 1.2
Γ_*	Γ_{*25} = 42.75 μmol mol^{-1} (4.3 Pa at 1,013.25 hPa)	ΔH_a = 37,830 J mol^{-1}	Γ_{*25} = 2.2 Pa (at 1,013.25 hPa)
Θ_{PSII}	0.7	-	-
f	0.15	-	-
Θ_{cj}	0.98	-	-
Θ_{ie}	0.95	-	-

calculated from $V_{c\ \max\ 25}^{opt}$ after adjustment for day length and nitrogen.

Appendix C: Canopy Integration

[60] *Thornton and Zimmermann* [2007] describe the CLM4 canopy integration parameterization, and *Oleson et al.* [2010] provide details of the numerical implementation. The leaf photosynthesis-conductance parameterization is solved separately for sunlit and shaded leaves using appropriate Rubisco carboxylation rates ($\overline{V}_{c\ \max\ 25}^{opt}$ (sun) and $\overline{V}_{c\ \max\ 25}^{opt}$ (sha), averaged for sunlit and shaded leaves, respectively) and absorbed photosynthetically active radiation (ϕ_{sun} and ϕ_{sha}) to calculate sunlit and shaded gross photosynthetic rates (A_{sun} and A_{sha}). Leaf temperature is not

Table B4. Equations for the C_4 Photosynthesis Model

Definition	PSN	CLM4
Rubisco-limited assimilation	$w_c = V_{c\ \max}$	same
Light-limited assimilation	$w_j = \varepsilon\ (4.6\phi)$ sunlit leaf : $\phi = \phi_{sun}$	same
CO_2-limited assimilation	$w_e = k_e\ c_i/P_{atm}$ shaded leaf : $\phi = \phi_{sha}$	same
Maximum carboxylation rate	$V_{c\max} = V_{c\ \max 25}\left[\frac{Q_{10}^{(T_v-298.15)/10}}{f_H(T_v) f_L(T_v)}\right]\beta_t$ $f_H(T_v) = 1 + \exp[s_1(T_v - s_2)]$ $f_L(T_v) = 1 + \exp[s_3(s_4 - T_v)]$ Q_{10} = 2; s_1 = 0.3 K^{-1}; s_2 = 313.15 K; s_3 = 0.2 K^{-1}; s_4 = 288.15 K; $V_{c\ \max\ 25}$ as for C_3 plants	$V_{c\ \max} = V_{c\ \max\ 25}\ [\frac{Q_{10}^{(T_v-298.15)/10}}{f_H(T_v)}]\beta_t$ $f_H\ (T_v) = 1 + \exp\ (\frac{\Delta S T_v - \Delta H_d}{R_{gas} T_v})$ Q_{10} = 2.4; ΔH_d = 220,000 J mol^{-1}; ΔS = 710 J mol^{-1} K^{-1}; $V_{c\ \max\ 25}$ as for C_3 plants
Initial slope CO_2 response curve	$k_e = k_{e25}\ Q_{10}^{(T_v\ -\ 298.15)/10}$ Q_{10} = 2; k_{e25} = 20,000 $V_{c\ \max\ 25}$	k_e = 4,000 $V_{c\ \max}$
Leaf dark respiration	$R_d = R_{d25}\ \{\frac{Q_{10}^{(T_v-298.15)/10}}{1+\exp[s_5(T_v-s_6)]}\}\beta_t$ Q_{10} = 2; s_5 = 1.3 K^{-1}; s_6 = 328.15K; R_{d25} = 0.025 $V_{c\ \max\ 25}$	-

distinguished between sunlit and shaded leaves. Canopy photosynthesis is $A_{sun}L_{sun} + A_{sha}L_{sha}$.

[61] In CLM4, $\overline{V}_{c\ \max\ 25}^{opt}$ is calculated for sunlit and shaded leaves from (B1) using the average specific leaf area (inverse of M_a) for sunlit and shaded leaves (M_a^{-1} equals $\overline{SLA}_{sun}$ for sunlit leaves and $\overline{SLA}_{sha}$ for shaded leaves). This canopy scaling keeps mass-based leaf nitrogen concentration N_m constant with depth in the canopy, but allows SLA to increase (M_a decreases) with greater cumulative leaf area index in the canopy so that $V_{c\ \max\ 25}^{opt}$ decreases with canopy depth. Specific leaf area increases linearly with greater cumulative leaf area index x ($m^2\ m^{-2}$) as

$$SLA(x) = SLA_0 + SLA_m x \tag{C1}$$

where SLA_0 is the specific leaf area at the top of the canopy and SLA_m is the slope coefficient. The average specific leaf area for sunlit leaves in a canopy with leaf area index L is

$$\begin{aligned}\overline{SLA}_{sun} &= \frac{\int_0^L SLA(x) f_{sun}(x)\,dx}{\int_0^L f_{sun}(x)\,dx} \\ &= \frac{SLA_m + SLA_0 K_b - [SLA_m(K_b L + 1) + SLA_0 K_b]e^{-K_b L}}{K_b^2 L_{sun}}\end{aligned} \tag{C2}$$

and for shaded leaves,

$$\begin{aligned}\overline{SLA}_{sha} &= \frac{\int_0^L SLA(x)[1 - f_{sun}(x)]\,dx}{\int_0^L [1 - f_{sun}(x)]\,dx} \\ &= \frac{SLA_0 L + 0.5 SLA_m L^2 - \overline{SLA}_{sun} L_{sun}}{L_{sha}}.\end{aligned} \tag{C3}$$

In this study, we calculate $\overline{V}_{c\ \max\ 25}^{opt}$ for sunlit and shaded leaves using an exponential profile to area-based leaf nitrogen N_a. $V_{c\ \max\ 25}^{opt}$ at cumulative leaf area index x from the canopy top scales directly with N_a, which decreases exponentially with greater cumulative leaf area, so that

$$V_{c\ \max 25}^{opt}(x) = V_{c\ \max 25}^{opt}(0) e^{-K_n x}. \tag{C4}$$

$V_{c\ \max\ 25}^{opt}$ (0) is defined at the top of the canopy from (B1) using M_a at the top of the canopy ($1/SLA_0$), and K_n is the decay coefficient for nitrogen. The canopy integrated value for sunlit and shaded leaves is

$$\begin{aligned}V_{c\ \max 25}^{opt}(\text{sun}) &= \int_0^L V_{c\ \max 25}^{opt}(x) f_{sun}(x)\,dx \\ &= V_{c\ \max 25}^{opt}(0)\left[1 - e^{-(K_n + K_b)L}\right]\frac{1}{K_n + K_b}\end{aligned} \tag{C5}$$

$$\begin{aligned}V_{c\ \max 25}^{opt}(\text{sha}) &= \int_0^L V_{c\ \max 25}^{opt}(x)[1 - f_{sun}(x)]\,dx \\ &= V_{c\ \max 25}^{opt}(0)\left\{\left[1 - e^{-K_n L}\right]\frac{1}{K_n} - \left[1 - e^{-(K_n + K_b)L}\right] \cdot \frac{1}{K_n + K_b}\right\}\end{aligned} \tag{C6}$$

and the average value for the sunlit and shaded leaves is

$$\overline{V}_{c\ \max 25}^{opt}(\text{sun}) = V_{c\ \max 25}^{opt}(\text{sun})/L_{sun} \tag{C7}$$

$$\overline{V}_{c\ \max 25}^{opt}(\text{sha}) = V_{c\ \max 25}^{opt}(\text{sha})/L_{sha}. \tag{C8}$$

Photosynthetic parameters $J_{\max\ 25}$, TPU_{25}, k_{e25}, and R_{d25} scale similarly. We use $K_n = 0.11$, derived by *Friend and Kiang* [2005] for the GISS model and used also in O-CN [*Zaehle and Friend*, 2010].

Notation

a_{R25}	specific activity of Rubisco at 25°C (μmol CO_2 g^{-1} Rubisco s^{-1}).
A	leaf gross photosynthesis rate (μmol CO_2 m^{-2} s^{-1}).
A_n	leaf net photosynthesis rate (μmol CO_2 m^{-2} s^{-1}).
b	minimum conductance for Ball-Berry model (μmol H_2O m^{-2} s^{-1}).
c_a	atmospheric CO_2 partial pressure (Pa).
c_i	intercellular CO_2 partial pressure (Pa).
c_s	CO_2 partial pressure at leaf surface (Pa).
D	day length (s).
$D_{\max}$	maximum day length (s).
e_a	vapor pressure of air (Pa).
e_s	vapor pressure at leaf surface (Pa).
$e_*\ [T_v]$	saturation vapor pressure at temperature T_v (Pa).
f	fraction of PAR absorbed by nonphotosynthetic materials.
f_{sun}	sunlit fraction of canopy.
$f(D)$	day length factor for $V_{c\ \max}$.
$f(N)$	nitrogen factor for $V_{c\ \max}$.
F_{LNR}	fraction of leaf nitrogen in Rubisco (g N [Rubisco] g^{-1} N [leaf]).
F_{NR}	mass ratio of Rubisco to nitrogen in Rubisco (g Rubisco g^{-1} N [Rubisco]).
g_b	leaf boundary layer conductance (μmol H_2O m^{-2} s^{-1}).
g_s	leaf stomatal conductance (μmol H_2O m^{-2} s^{-1}).
h	*Oleson et al.* [2010, equation (3.25)].
$h_1 - h_{10}$	*Oleson et al.* [2010, equations (3.38)–(3.47)].
h_s	leaf surface humidity (fraction).
$I\uparrow_\Lambda$	upward scattered flux per unit diffuse flux [*Oleson et al.*, 2010, equation (3.18)].
$I\uparrow_\Lambda^\mu$	upward scattered flux per unit direct beam flux [*Oleson et al.*, 2010, equation (3.17)].
$I\downarrow_\Lambda$	downward scattered flux per unit diffuse flux [*Oleson et al.*, 2010, equation (3.20)].
$I\downarrow_\Lambda^\mu$	downward scattered flux per unit direct beam flux [*Oleson et al.*, 2010, equation (3.19)].

$\vec{I}_\Lambda$ diffuse radiation absorbed by the canopy per unit diffuse flux.
$\vec{I}^{\mu}_\Lambda$ direct beam radiation absorbed by the canopy per unit direct beam flux.
$\vec{I}_{sha,\Lambda}$ diffuse radiation absorbed by shaded leaves per unit diffuse flux.
$\vec{I}^{\mu}_{sha,\Lambda}$ direct beam radiation absorbed by shaded leaves per unit direct beam flux.
$\vec{I}^{tot}_{sha,\Lambda}$ total solar radiation absorbed by shaded leaves (W m^{-2} [ground]).
$\vec{I}_{sun,\Lambda}$ diffuse radiation absorbed by sunlit leaves per unit diffuse flux.
$\vec{I}^{\mu}_{sun,\Lambda}$ direct beam radiation absorbed by sunlit leaves per unit direct beam flux.
$\vec{I}^{tot}_{sun,\Lambda}$ total solar radiation absorbed by sunlit leaves (W m^{-2} [ground]).
$I_{lb,\Lambda}$ leaf absorbed direct beam radiation (W m^{-2} [leaf]).
$I_{lbs,\Lambda}$ leaf absorbed scattered direct beam radiation (W m^{-2} [leaf]).
$I_{ld,\Lambda}$ leaf absorbed diffuse radiation (W m^{-2} [leaf]).
I_{PSII} photosynthetically active radiation absorbed by PS II (μmol photon m^{-2} s^{-1}).
J electron transport rate (μmol electron m^{-2} s^{-1}).
$J_{\max}$ maximum electron transport rate (μmol electron m^{-2} s^{-1}).
$J_{\max\ 25}$ $J_{\max}$ at 25°C.
k_e initial slope of C_4 CO_2 response curve (μmol m^{-2} s^{-1}).
k_{e25} k_e at 25°C.
K_b direct beam extinction coefficient [*Oleson et al.*, 2010, equation (4.8)].
K_c Michaelis-Menten constant for CO_2 (Pa).
K_{c25} K_c at 25°C.
K_n foliage nitrogen decay coefficient.
K_o Michaelis-Menten constant for O_2 (Pa).
K_{o25} K_o at 25°C.
L' vegetation area index, $L + S$ (m^2 m^{-2}).
L leaf area index (m^2 m^{-2}).
L_{sha} shaded leaf area index (m^2 m^{-2}).
L_{sun} sunlit leaf area index (m^2 m^{-2}).
m slope of Ball-Berry model.
M_a leaf mass per unit area (g C [leaf] m^{-2} [leaf]).
N_a area-based leaf nitrogen (g N [leaf] m^{-2} [leaf]).
N_m mass-based leaf nitrogen (g N [leaf] g^{-1} C [leaf]).
o_i intercellular O_2 partial pressure (Pa).
P_{atm} atmospheric pressure (Pa).
Q_{10} Q10 temperature parameter.
R_d leaf "dark," or "day," respiration rate (μmol CO_2 m^{-2} s^{-1}).
R_{d25} R_d at 25°C.
R_{gas} gas constant (8.314 J K^{-1} mol^{-1}).
s_1, s_2 *Oleson et al.* [2010, equations (3.30) and (3.31)].
S stem area index (m^2 m^{-2}).
$S_{atm}\downarrow_\Lambda$ incident diffuse radiation above the canopy (W m^{-2} [ground]).
$S_{atm}\downarrow^{\mu}_\Lambda$ incident direct beam radiation above the canopy (W m^{-2} [ground]).
SLA specific leaf area (m^2 [leaf] g^{-1} C [leaf]).
$\overline{SLA}$ average SLA for sunlit or shaded leaves.
SLA_0 SLA at the top of the canopy.
SLA_m SLA linear slope coefficient.
T_v leaf temperature (K).
TPU triose phosphate utilization rate (μmol m^{-2} s^{-1}).
TPU_{25} TPU at 25°C.
$V_{c\ \max}$ maximum Rubisco carboxylation rate (μmol m^{-2} s^{-1}).
$V_{c\ \max\ 25}$ $V_{c\ \max}$ at 25°C.
$V_c^{\ opt}{}_{\max\ 25}$ potential $V_{c\ \max\ 25}$, without day length factor $f(D)$ and nitrogen factor $f(N)$.
$\overline{V}_c^{\ opt}{}_{\max\ 25}$ average $V_c^{\ opt}{}_{\max\ 25}$ for sunlit or shaded leaves.
w_c Rubisco-limited assimilation rate (μmol CO_2 m^{-2} s^{-1}).
w_e export-limited (C_3) or CO_2-limited (C_4) assimilation rate (μmol CO_2 m^{-2} s^{-1}).
w_i intermediate colimited assimilation rate (μmol CO_2 m^{-2} s^{-1}).
w_j light-limited assimilation rate (μmol CO_2 m^{-2} s^{-1}).
x cumulative leaf area index from canopy top (m^2 m^{-2}).
β_t CLM4 soil water stress [*Oleson et al.*, 2010, equation (8.17)].
Γ_* CO_2 compensation point in the absence of non-photorespiratory respiration (Pa).
Γ_{*25} Γ_* at 25°C.
ΔH_a activation energy (J mol^{-1}).
ΔH_d deactivation energy (J mol^{-1}).
ΔS entropy term (J K^{-1} mol^{-1}).
ε quantum yield (mol CO_2 mol^{-1} photon).
Θ_{cj} curvature factor for photosynthesis colimitation.
Θ_{ie} curvature factor for photosynthesis colimitation.
Θ_{PSII} curvature factor for electron transport.
$\overline{\mu}$ *Oleson et al.* [2010, equation (3.4)].
σ *Oleson et al.* [2010, equation (3.26)].
ϕ average absorbed PAR for sunlit ϕ_{sun} or shaded ϕ_{sha} leaf (W m^{-2} [leaf]).
ω_Λ leaf scattering coefficient [*Oleson et al.*, 2010, equation (3.5)].

[62] **Acknowledgment.** The National Center for Atmospheric Research is sponsored by the National Science Foundation.

References

Alton, P., L. Mercado, and P. North (2007), A sensitivity analysis of the land-surface scheme JULES conducted for three forest biomes: Biophysical parameters, model processes, and meteorological driving data, *Global Biogeochem. Cycles*, *20*, GB1008, doi:10.1029/2005GB002653.

Anten, N. P. R., F. Schieving, and M. J. A. Werger (1998), Nitrogen distribution and leaf area indices in relation to photosynthetic nitrogen use efficiency in savanna grasses, *Plant Ecol.*, *138*, 63–75, doi:10.1023/A:1009727822617.

Aubinet, M. A., et al. (2000), Estimates of the annual net carbon and water exchange of forests: The EUROFLUX methodology, *Adv. Ecol. Res*, *30*, 113–175, doi:10.1016/S0065-2504(08)60018-5.

Baldocchi, D. D., and K. B. Wilson (2001), Modeling CO_2 and water vapor exchange of a temperate broadleaved forest across hourly to decadal time scales, *Ecol. Modell.*, *142*, 155–184, doi:10.1016/S0304-3800(01)00287-3.

Baldocchi, D. D., K. B. Wilson, and L. Gu (2002), How the environment, canopy structure and canopy physiological functioning influence carbon, water and energy fluxes of a temperate broad-leaved deciduous forest—An assessment with the biophysical model CANOAK, *Tree Physiol.*, *22*, 1065–1077.

Ball, J. T., I. E. Woodrow, and J. A. Berry (1987), A model predicting stomatal conductance and its contribution to the control of photosynthesis under different environmental conditions, in *Progress in Photosynthesis*

Research, vol. 4, edited by J. Biggins, pp. 221–224, Martinus Nijhoff, Dordrecht, Netherlands.

Beer, C., et al. (2010), Terrestrial gross carbon dioxide uptake: Global distribution and covariation with climate, *Science*, *329*, 834–838, doi:10.1126/science.1184984.

Beerling, D. J., and W. P. Quick (1995), A new technique for estimating rates of carboxylation and electron transport in leaves of C_3 plants for use in dynamic global vegetation models, *Global Change Biol.*, *1*, 289–294, doi:10.1111/j.1365-2486.1995.tb00027.x.

Bernacchi, C. J., E. L. Singsaas, C. Pimentel, A. R. Portis Jr., and S. P. Long (2001), Improved temperature response functions for models of Rubisco-limited photosynthesis, *Plant Cell Environ.*, *24*, 253–259, doi:10.1111/j.1365-3040.2001.00668.x.

Bernacchi, C. J., C. Pimentel, and S. P. Long (2003), In vivo temperature response functions of parameters required to model RuBP-limited photosynthesis, *Plant Cell Environ.*, *26*, 1419–1430, doi:10.1046/j.0016-8025.2003.01050.x.

Bonan, G. B. (1995), Land-atmosphere CO_2 exchange simulated by a land surface process model coupled to an atmospheric general circulation model, *J. Geophys. Res.*, *100*, 2817–2831, doi:10.1029/94JD02961.

Bonan, G. B. (1996), A land surface model (LSM version 1.0) for ecological, hydrological, and atmospheric studies: Technical description and user's guide, *NCAR Tech. Note NCAR/TN-417+STR*, 150 pp., Natl. Cent. for Atmos. Res., Boulder, Colo.

Bonan, G. B. (2008), Forests and climate change: Forcings, feedbacks, and the climate benefits of forests, *Science*, *320*, 1444–1449, doi:10.1126/science.1155121.

Bonan, G. B., and S. Levis (2010), Quantifying carbon-nitrogen feedbacks in the Community Land Model (CLM4), *Geophys. Res. Lett.*, *37*, L07401, doi:10.1029/2010GL042430.

Bonan, G. B., K. W. Oleson, M. Vertenstein, S. Levis, X. Zeng, Y. Dai, R. E. Dickinson, and Z.-L. Yang (2002), The land surface climatology of the Community Land Model coupled to the NCAR Community Climate Model, *J. Clim.*, *15*, 3123–3149, doi:10.1175/1520-0442(2002)015<3123:TLSCOT>2.0.CO;2.

Carswell, F. E., P. Meir, E. V. Wandelli, L. C. M. Bonates, B. Kruijt, E. M. Barbosa, A. D. Nobre, J. Grace, and P. G. Jarvis (2000), Photosynthetic capacity in a central Amazonian rain forest, *Tree Physiol.*, *20*, 179–186.

Chen, H., R. E. Dickinson, Y. Dai, and L. Zhou (2010), Sensitivity of simulated terrestrial carbon assimilation and canopy transpiration to different stomatal conductance and carbon assimilation schemes, *Clim. Dyn.*, doi:10.1007/00382-00010-00741-00382.

Collatz, G. J., J. T. Ball, C. Grivet, and J. A. Berry (1991), Physiological and environmental regulation of stomatal conductance, photosynthesis and transpiration: A model that includes a laminar boundary layer, *Agric. For. Meteorol.*, *54*, 107–136, doi:10.1016/0168-1923(91)90002-8.

Collatz, G. J., M. Ribas-Carbo, and J. A. Berry (1992), Coupled photosynthesis-stomatal conductance model for leaves of C_4 plants, *Aust. J. Plant Physiol.*, *19*, 519–538, doi:10.1071/PP9920519.

Dai, Y., R. E. Dickinson, and Y.-P. Wang (2004), A two-big-leaf model for canopy temperature, photosynthesis, and stomatal conductance, *J. Clim.*, *17*, 2281–2299.

Dang, Q.-L., H. A. Margolis, and G. J. Collatz (1998), Parameterization and testing of a coupled photosynthesis-stomatal conductance model for boreal trees, *Tree Physiol.*, *18*, 141–153.

de Pury, D. G. G., and G. D. Farquhar (1997), Simple scaling of photosynthesis from leaves to canopies without the errors of big-leaf models, *Plant Cell Environ.*, *20*, 537–557, doi:10.1111/j.1365-3040.1997.00094.x.

Dickinson, R. E., K. W. Oleson, G. Bonan, F. Hoffman, P. Thornton, M. Vertenstein, Z.-L. Yang, and X. Zeng (2006), The Community Land Model and its climate statistics as a component of the Community Climate System Model, *J. Clim.*, *19*, 2302–2324, doi:10.1175/JCLI3742.1.

Drecger, M. F., M. van Oijen, A. H. C. M. Schapendonk, C. S. Pot, and R. Rabbinge (2000), Dynamics of vertical leaf nitrogen distribution in a vegetative wheat canopy. Impact on canopy photosynthesis, *Ann. Bot.*, *86*, 821–831, doi:10.1006/anbo.2000.1244.

Drouet, J.-L., and R. Bonhomme (2004), Effect of 3D nitrogen, dry mass per area and local irradiance on canopy photosynthesis within leaves of contrasted heterogeneous maize crops, *Ann. Bot.*, *93*, 699–710, doi:10.1093/aob/mch099.

Ellsworth, D. S., and P. B. Reich (1993), Canopy structure and vertical patterns of photosynthesis and related leaf traits in a deciduous forest, *Oecologia*, *96*, 169–178, doi:10.1007/BF00317729.

Evans, J. R. (1993), Photosynthetic acclimation and nitrogen partitioning within a lucerne canopy. I. Canopy characteristics, *Aust. J. Plant Physiol.*, *20*, 55–67, doi:10.1071/PP9930055.

Farquhar, G. D., S. von Caemmerer, and J. A. Berry (1980), A biochemical model of photosynthetic CO_2 assimilation in leaves of C_3 species, *Planta*, *149*, 78–90, doi:10.1007/BF00386231.

Friedlingstein, P., et al. (2006), Climate-carbon cycle feedback analysis: Results from the C^4MIP model intercomparison, *J. Clim.*, *19*, 3337–3353, doi:10.1175/JCLI3800.1.

Friend, A. D., and N. Y. Kiang (2005), Land surface model development for the GISS GCM: Effects of improved canopy physiology on simulated climate, *J. Clim.*, *18*, 2883–2902, doi:10.1175/JCLI3425.1.

Friend, A. D., et al. (2007), FLUXNET and modelling the global carbon cycle, *Global Change Biol.*, *13*, 610–633, doi:10.1111/j.1365-2486.2006.01223.x.

Gastal, F., and G. Lemaire (2002), N uptake and distribution in crops: An agronomical and ecophysiological perspective, *J. Exp. Bot.*, *53*, 789–799, doi:10.1093/jexbot/53.370.789.

Goudriaan, J. (1977), Crop micrometeorology: A simulation study, 249 pp., Cent. for Agric. Publ. Doc., Wageningen, Netherlands.

Goudriaan, J., and H. H. van Laar (1994), *Modelling Potential Crop Growth Processes: Textbook With Exercises*, 238 pp., Kluwer Acad., Dordrecht, Netherlands.

Grassi, G., E. Vicinelli, F. Ponti, L. Cantoni, and F. Magnani (2005), Seasonal and interannual variability of photosynthetic capacity in relation to leaf nitrogen in a deciduous forest plantation in northern Italy, *Tree Physiol.*, *25*, 349–360.

Harley, P. C., and T. D. Sharkey (1991), An improved model of C_3 photosynthesis at high CO_2: Reversed O_2 sensitivity explained by lack of glycerate reentry into the chloroplast, *Photosynth. Res.*, *27*, 169–178.

Harley, P. C., R. B. Thomas, J. F. Reynolds, and B. R. Strain (1992), Modelling photosynthesis of cotton grown in elevated CO_2, *Plant Cell Environ.*, *15*, 271–282, doi:10.1111/j.1365-3040.1992.tb00974.x.

Hirose, T., and M. J. A. Werger (1987), Maximizing daily canopy photosynthesis with respect to the leaf nitrogen allocation pattern in the canopy, *Oecologia*, *72*, 520–526, doi:10.1007/BF00378977.

Hirose, T., M. J. A. Werger, T. L. Pons, and J. W. A. van Rheenen (1988), Canopy structure and leaf nitrogen distribution in a stand of *Lysimachia vulgaris* L. as influenced by stand density, *Oecologia*, *77*, 145–150, doi:10.1007/BF00379180.

Hollinger, D. Y. (1996), Optimality and nitrogen allocation in a tree canopy, *Tree Physiol.*, *16*, 627–634.

Jung, M., M. Reichstein, and A. Bondeau (2009), Towards global empirical upscaling of FLUXNET eddy covariance observations: Validation of a model tree ensemble approach using a biosphere model, *Biogeosciences*, *6*, 2001–2013, doi:10.5194/bg-6-2001-2009.

Jung, M., et al. (2010), Recent decline in the global land evapotranspiration trend due to limited moisture supply, *Nature*, *467*, 951–954, doi:10.1038/nature09396.

Kattge, J., W. Knorr, T. Raddatz, and C. Wirth (2009), Quantifying photosynthetic capacity and its relationship to leaf nitrogen content for global-scale terrestrial biosphere models, *Global Change Biol.*, *15*, 976–991, doi:10.1111/j.1365-2486.2008.01744.x.

Kosugi, Y., S. Shibata, and S. Kobashi (2003), Parameterization of the CO_2 and H_2O gas exchange of several temperate deciduous broad-leaved trees at the leaf scale considering seasonal changes, *Plant Cell Environ.*, *26*, 285–301, doi:10.1046/j.1365-3040.2003.00960.x.

Kowalczyk, E. A., Y. P. Wang, R. M. Law, H. L. Davies, J. L. McGregor, and G. Abramowitz (2006), The CSIRO Atmosphere Biosphere Land Exchange (CABLE) model for use in climate models and as an offline model, *Pap. 013*, 37 pp., CSIRO Mar. Atmos. Res., Aspendale, Vic., Australia.

Lasslop, G., M. Reichstein, D. Papale, A. D. Richardson, A. Arneth, A. Barr, P. Stoy, and G. Wohlfahrt (2010), Separation of net ecosystem exchange into assimilation and respiration using a light response curve approach: Critical issues and global evaluation, *Global Change Biol.*, *16*, 187–208, doi:10.1111/j.1365-2486.2009.02041.x.

Lawrence, D. M., et al. (2011), Parameterization improvements and functional and structural advances in version 4 of the Community Land Model, *J. Adv. Model. Earth Syst.*, *3*, M03001, doi:10.1029/2011MS000045.

Leuning, R. (2002), Temperature dependence of two parameters in a photosynthesis model, *Plant Cell Environ.*, *25*, 1205–1210, doi:10.1046/j.1365-3040.2002.00898.x.

Lloyd, J., et al. (2010), Optimisation of photosynthetic carbon gain and within-canopy gradients of associated foliar traits for Amazon forest trees, *Biogeosciences*, *7*, 1833–1859, doi:10.5194/bg-7-1833-2010.

Luyssaert, S., et al. (2007), CO_2 balance of boreal, temperate, and tropical forests derived from a global database, *Global Change Biol.*, *13*, 2509–2537, doi:10.1111/j.1365-2486.2007.01439.x.

Mahecha, M. D., et al. (2010), Comparing observations and process-based simulations of biosphere-atmosphere exchanges on multiple timescales, *J. Geophys. Res.*, *115*, G02003, doi:10.1029/2009JG001016.

Meir, P., B. Kruijt, M. Broadmeadow, E. Barbosa, O. Kull, F. Carswell, A. Nobre, and P. G. Jarvis (2002), Acclimation of photosynthetic capac-

ity to irradiance in tree canopies in relation to leaf nitrogen concentration and leaf mass per unit area, *Plant Cell Environ.*, *25*, 343–357, doi:10.1046/j.0016-8025.2001.00811.x.

Mercado, L., J. Lloyd, F. Carswell, Y. Malhi, P. Meir, and A. D. Nobre (2006), Modelling Amazonian forest eddy covariance data: A comparison of big leaf versus sun/shade models for the C-14 tower at Manus. I. Canopy photosynthesis, *Acta Amazon.*, *36*, 69–82, doi:10.1590/S0044-59672006000100009.

Mercado, L. M., J. Lloyd, A. J. Dolman, S. Sitch, and S. Patiño (2009a), Modelling basin-wide variations in Amazon forest productivity—Part 1: Model calibration, evaluation and upscaling functions for canopy photosynthesis, *Biogeosciences*, *6*, 1247–1272, doi:10.5194/bg-6-1247-2009.

Mercado, L. M., N. Bellouin, S. Sitch, O. Boucher, C. Huntingford, M. Wild, and P. M. Cox (2009b), Impact of changes in diffuse radiation on the global land carbon sink, *Nature*, *458*, 1014–1017, doi:10.1038/nature07949.

Morales, P., et al. (2005), Comparing and evaluating process-based ecosystem model predictions of carbon and water fluxes in major European forest biomes, *Global Change Biol.*, *11*, 2211–2233, doi:10.1111/j.1365-2486.2005.01036.x.

Niinemets, Ü. (2007), Photosynthesis and resource distribution through plant canopies, *Plant Cell Environ.*, *30*, 1052–1071, doi:10.1111/j.1365-3040.2007.01683.x.

Niinemets, Ü., and J. D. Tenhunen (1997), A model separating leaf structural and physiological effects on carbon gain along light gradients for the shade-tolerant species *Acer saccharum*, *Plant Cell Environ.*, *20*, 845–866, doi:10.1046/j.1365-3040.1997.d01-133.x.

Niinemets, Ü., W. Bilger, O. Kull, and J. D. Tenhunen (1999), Responses of foliar photosynthetic electron transport, pigment stoichiometry, and stomatal conductance to interacting environmental factors in a mixed species forest canopy, *Tree Physiol.*, *19*, 839–852.

Norman, J. M. (1979), Modeling the complete crop canopy, in *Modification of the Aerial Environment of Plants*, edited by B. J. Barfield and J. F. Gerber, pp. 249–277, Am. Soc. of Agric. Eng., St. Joseph, Mich.

Oleson, K. W., et al. (2004), Technical description of the Community Land Model (CLM), *NCAR Tech. Note NCAR/TN-461+STR*, 173 pp., Natl. Cent. for Atmos. Res., Boulder, Colo.

Oleson, K. W., et al. (2008), Improvements to the Community Land Model and their impact on the hydrological cycle, *J. Geophys. Res.*, *113*, G01021, doi:10.1029/2007JG000563.

Oleson, K. W., et al. (2010), Technical description of version 4.0 of the Community Land Model (CLM), *NCAR Tech. Note NCAR/TN-478+STR*, 257 pp., Natl. Cent. for Atmos. Res., Boulder, Colo.

Ow, L. F., D. Whitehead, A. S. Walcroft, and M. H. Turnbull (2010), Seasonal variation in foliar carbon exchange in *Pinus radiata* and *Populus deltoides*: Respiration acclimates fully to changes in temperature but photosynthesis does not, *Global Change Biol.*, *16*, 288–302, doi:10.1111/j.1365-2486.2009.01892.x.

Randerson, J. T., et al. (2009), Systematic assessment of terrestrial biogeochemistry in coupled climate-carbon models, *Global Change Biol.*, *15*, 2462–2484, doi:10.1111/j.1365-2486.2009.01912.x.

Schimel, D. S., T. G. F. Kittel, A. K. Knapp, T. R. Seastedt, W. J. Parton, and V. B. Brown (1991), Physiological interactions along resource gradients in a tallgrass prairie, *Ecology*, *72*, 672–684, doi:10.2307/2937207.

Sellers, P. J., J. A. Berry, G. J. Collatz, C. B. Field, and F. G. Hall (1992), Canopy reflectance, photosynthesis, and transpiration. III. A reanalysis using improved leaf models and a new canopy integration scheme, *Remote Sens. Environ.*, *42*, 187–216, doi:10.1016/0034-4257(92)90102-P.

Sellers, P. J., D. A. Randall, G. J. Collatz, J. A. Berry, C. B. Field, D. A. Dazlich, C. Zhang, G. D. Collelo, and L. Bounoua (1996a), A revised land surface parameterization (SiB2) for atmospheric GCMs. Part I: Model formulation, *J. Clim.*, *9*, 676–705, doi:10.1175/1520-0442(1996)009<0676:ARLSPF>2.0.CO;2.

Sellers, P. J., S. O. Los, C. J. Tucker, C. O. Justice, D. A. Dazlich, G. J. Collatz, and D. A. Randall (1996b), A revised land surface parameterization (SiB2) for atmospheric GCMs. Part II: The generation of global fields of terrestrial biophysical parameters from satellite data, *J. Clim.*, *9*, 706–737, doi:10.1175/1520-0442(1996)009<0706:ARLSPF>2.0.CO;2.

Stöckli, R., D. M. Lawrence, G.-Y. Niu, K. W. Oleson, P. E. Thornton, Z.-L. Yang, G. B. Bonan, A. S. Denning, and S. W. Running (2008), Use of FLUXNET in the Community Land Model development, *J. Geophys. Res.*, *113*, G01025, doi:10.1029/2007JG000562.

Thornton, P. E., and N. E. Zimmermann (2007), An improved canopy integration scheme for a land surface model with prognostic canopy structure, *J. Clim.*, *20*, 3902–3923, doi:10.1175/JCLI4222.1.

von Caemmerer, S. (2000), Biochemical models of leaf photosynthesis, 165 pp., CSIRO, Collingwood, Vic., Australia.

Wang, Q., J. Tenhunen, E. Falge, C. Bernhofer, and A. Granier (2003), Simulation and scaling of temporal variation in gross primary production for coniferous and deciduous temperate forests, *Global Change Biol.*, *10*, 37–51, doi:10.1111/j.1365-2486.2003.00716.x.

Wang, Q., A. Iio, J. Tenhunen, and Y. Kakubari (2008), Annual and seasonal variations in photosynthetic capacity of *Fagus crenata* along an elevation gradient in the Naeba Mountains, Japan, *Tree Physiol.*, *28*, 277–285.

Wang, Q., J. Tenhunen, and T. Vesala (2009a), Correlated change in normalized difference vegetation index and the seasonal trajectory of photosynthetic capacity in a conifer stand, *Int. J. Remote Sens.*, *30*, 983–1001, doi:10.1080/01431160802427905.

Wang, Q., J. Tenhunen, and T. Vesala (2009b), Gross primary production simulation in a coniferous forest using a daily gas exchange model with seasonal change of leaf physiological parameters derived from remote sensing data, *Int. J. Remote Sens.*, *30*, 3013–3025, doi:10.1080/01431160802558691.

Wang, Y.-P., and R. Leuning (1998), A two-leaf model for canopy conductance, photosynthesis and partitioning of available energy. I: Model description and comparison with a multi-layered model, *Agric. For. Meteorol.*, *91*, 89–111, doi:10.1016/S0168-1923(98)00061-6.

Williams, M., et al. (2009), Improving land surface models with FLUXNET data, *Biogeosciences*, *6*, 1341–1359, doi:10.5194/bg-6-1341-2009.

Wilson, K. B., D. D. Baldocchi, and P. J. Hanson (2000), Spatial and seasonal variability of photosynthetic parameters and their relationship to leaf nitrogen in a deciduous forest, *Tree Physiol.*, *20*, 565–578.

Wilson, K. B., D. D. Baldocchi, and P. J. Hanson (2001), Leaf age affects the seasonal pattern of photosynthetic capacity and net ecosystem exchange of carbon in a deciduous forest, *Plant Cell Environ.*, *24*, 571–583, doi:10.1046/j.0016-8025.2001.00706.x.

Wittig, V. E., et al. (2005), Gross primary production is stimulated for three *Populus* species grown under free-air CO_2 enrichment from planting through canopy closure, *Global Change Biol.*, *11*, 644–656, doi:10.1111/j.1365-2486.2005.00934.x.

Wullschleger, S. D. (1993), Biochemical limitations to carbon assimilation in C_3 plants—A retrospective analysis of the A/C_i curves from 109 species, *J. Exp. Bot.*, *44*, 907–920, doi:10.1093/jxb/44.5.907.

Xu, L., and D. D. Baldocchi (2003), Seasonal trends in photosynthetic parameters and stomatal conductance of blue oak (*Quercus douglasii*) under prolonged summer drought and high temperature, *Tree Physiol.*, *23*, 865–877.

Zaehle, S., and A. D. Friend (2010), Carbon and nitrogen cycle dynamics in the O-CN land surface model: 1. Model description, site-scale evaluation, and sensitivity to parameter estimates, *Global Biogeochem. Cycles*, *24*, GB1005, doi:10.1029/2009GB003521.

G. B. Bonan, D. M. Lawrence, P. J. Lawrence, S. Levis, K. W. Oleson, and S. C. Swenson, National Center for Atmospheric Research, PO Box 3000, 1850 Table Mesa Dr., Boulder, CO 80307-3000, USA. (bonan@ucar.edu)

M. Jung and M. Reichstein, Max Planck Institute for Biogeochemistry, D-07745 Jena, Germany.